

REVIEWS OF TOPICAL PROBLEMS PACS numbers: 41.75.Jv, 52.38.Kd, **87.50.–a**, 87.53.Jw, **87.55.–x**, **87.56.–v**

Laser ion acceleration for hadron therapy

S V Bulanov, J J Wilkens, T Zh Esirkepov, G Korn,
G Kraft, S D Kraft, M Molls, V S Khoroshkov

DOI: 10.3367/UFNe.0184.201412a.1265

Contents

Abstract. **The paper examines the prospects of using laser plasma as a source of high-energy ions for the purpose of hadron beam therapy — an approach which is based on both theory and experimental results (ions are routinely observed to be accelerated in the interaction of high-power laser radiation with matter). Compared to therapy accelerators like synchrotrons and cyclotrons, laser technology is advantageous in that it is more compact and is simpler in delivering ions from the accelerator to the treatment room. Special target designs allow radiation therapy requirements for ion beam quality to be satisfied.**

1. Introduction

Oncological morbidity and mortality are still pressing problems of contemporary medicine, despite substantial progress in malignant tumor diagnosis and treatment. At the end of the first decade of the 21st century, the five-year

S V Bulanov Prokhorov General Physics Institute, Russian Academy of Sciences, ul. Vavilova 38, 119991 Moscow, Russian Federation;
Moscow Institute of Physics and Technology (State University), Institutskii per. 9, 141700 Dolgoprudnyi, Moscow region, Russian Federation;
Advanced Beam Technology Division, Japan Atomic Energy Agency, 8-1-7 Umemidai, Kizugawa-shi, Kyoto-fu 619-0215, Japan
Tel. +81 774-71-3005. Fax +81 774-71-3316
E-mail: bulanov.sergei@jaea.go.jp
J J Wilkens, M Molls Klinikum rechts der Isar, Technische Universität München, Department of Radiation Oncology, Ismaninger Str. 22, 81675 München, Germany
Tel. +49 89 4140-4504. Fax +49 89 4140-4881
E-mail: wilkens@tum.de, molls@lrz.tum.de; www.radonc.med.tum.de
T Zh Esirkepov Moscow Institute of Physics and Technology (State University), Institutskii per. 9, 141700 Dolgoprudnyi, Moscow region, Russian Federation;
Advanced Beam Technology Division, Japan Atomic Energy Agency, 8-1-7 Umemidai, Kizugawa-shi, Kyoto-fu 619-0215, Japan
Tel. +81 774-71-3393. Fax +81 774-71-3316
E-mail: timur.esirkepov@jaea.go.jp
G Korn ELI-Beamlines, Institute of Physics, Czech Republic Academy of Sciences, Na Slovance 2, 182 21 Prague 8, Czech Republic
Tel. +420 26605-1315, +420 26605-1316
E-mail: Georg.Korn@eli-beams.eu
G Kraft Gesellschaft für Schwerionenforschung GmbH, Planckstr. 1, 6100 Darmstadt, Germany
S D Kraft Research Center Dresden-Rossendorf (FZD), P.O. Box 510119, 01314 Dresden, Germany
E-mail: s.kraft@hzdr.de
V S Khoroshkov Alikhanov Institute for Theoretical and Experimental Physics, ul. B. Cheremushkinskaya 25, 117218 Moscow, Russian Federation
Tel. +7 (499) 123 80 92
Fax +7 (499) 125 58 06
E-mail: khoroshkov@itep.ru

Received 3 March 2014
Uspekhi Fizicheskikh Nauk **184** (12) 1265 – 1298 (2014)
DOI: 10.3367/UFNr.0184.201412a.1265
Translated by S V Bulanov; edited by A Radzig

post-treatment recurrence-free survival rate (the rate of practical recovery) for patients diagnosed with cancer exceeded 60%, compared to 5% at the beginning of the 20th century. The possibility of a favorable prognosis depends on the type of disease. Early stages of Hodgkin's disease, larynx cancer, and childhood leukemia are treatable. For some other diseases, such as pancreatic cancer, the prognosis is less hopeful.

Here, 'recovery' means the absence of recurrence and/or metastasis, i.e., no manifestations of the same disease in the course of five years. Notwithstanding the high survival rates, the oncological mortality at present is decreasing rather slowly. This is mainly due to steady growth of the number of diagnosed cancer cases related to environmental deterioration and other contributing factors, increasing life expectancy, and the improvement in the early detection of cancer.

Cancers are a large family of different diseases affecting practically all the organs of the human body. Cancer appears at the cell level, as a result of a few, usually three, consecutive mutations [1]. The conclusion about several mutations is based on the known exponential dependence of the cancer probability on age. Otherwise, if a single mutation was able to turn healthy cells into cancerous ones, the probability of the disease would not depend on age. As a result of such a transformation, the affected cells start to replicate uncontrollably. In a normal situation, for example, red blood cells, erythrocytes, produced by bone marrow have a finite lifetime (about 100 days). Cell death, apoptosis, is programmed at the DNA (deoxyribonucleic acid) level. If for some reasons the apoptosis turns off, the erythrocyte lifetime substantially increases, leading to one form of erythroleukemia. Cells division is slow in some organs of the healthy adult human, e.g., in the cerebrum. After the neoplastic transformation of normal cells into cancer cells, their quick division produces malignant tumors surrounded by a developed system of blood vessels. At a late stage, cancer cells spread throughout the body with blood and lymph flows, creating secondary tumors called metastasis.

A great complication stems from the fact that cancers occur in forms that are difficult to treat. Malignant tumors typically possess a complex shape with numerous appendices; this is why it is called 'cancer' — 'crab' *in Latin*. The complication of the shape is already seen at the cellular level: cancer cells, unlike healthy ones, have a fractal structure [2]. As is well known, there is a connection between fractals and percolation processes. It is possible that a complex shape peculiar to tumors results from the fact that their fast growth with a penetration into healthy tissue is of the nature of percolation.

Cancers are often localized in close proximity to vital anatomical organs. In cases when the tumor has a compact form and is confined in a relatively small volume, one can prescribe surgery, radiation surgery, and/or radiation therapy. When the malignant tumor occupies a considerable volume with a complex shape, its surgical removal does not seem to be optimal. In this case, radiotherapy and chemotherapy offer a better way of the cancer treatment [3].

Radiotherapy uses not only high-energy ions but also π-mesons, neutrons, electrons, X-rays, and gamma-rays (for details, see Refs [4–14] and the literature cited therein). Hadron therapy represents a part of radiation therapy. For irradiation of malignant tumors, it uses fast charged particles with a high mass, such as protons and heavier ions.

In the approaches adopted in developed countries to cure cancer, which show the highest recovery level of cancer patients, all three complementary methods are utilized: surgery, radiotherapy, and chemotherapy. First, the bulk of the malignant tumor is removed by surgery, then radiation therapy destroys residual cancer cells at the periphery of the initial localization of the tumor, and, finally, chemotherapy kills cancer cells which could spread throughout the body. At the early stages of the disease, a successful treatment is often possible with only the first two local methods.

Apparently, a higher efficacy of cancer cell killing might be reached with greater doses of drugs with chemotherapy, more aggressive surgery, or higher levels of irradiation with radiotherapy. However, the cost of such treatment would be unacceptably high because of intolerable damage to normal tissues.

The hazardous effects of radiation therapy are associated with the risk of secondary cancer and/or serious postradiation complications due to the inevitable irradiation of healthy tissues. For this reason, the goal of radiation therapy consists in delivering a high enough dose to the malignant tumor, while sparing the surrounding tissues and nearby organs.

The requirement of a low level of exposure of nearby tissues and organs is of particular importance in childhood oncology. On the one hand, the probability of successful treatment of pediatric cancers is high, about 80%. On the other hand, the probability of secondary tumors as a result of radiation therapy is higher for children than for adults, because children's bodies are in the stage of growth, accompanied by cell differentiation [15]. In addition, the risk of secondary tumors is significant due to the higher life expectancy of children. Hadron therapy has an undoubted advantage in childhood oncology. As an example, we present in Table 1 data on the probability of secondary tumors resulting from the treatment of cerebellar medulloblastoma with X-ray radiation therapy or with proton therapy [16, 17].

Table 1. Secondary tumor probability resulting from the treatment of cerebellar medulloblastoma* with gamma-ray therapy as compared to treatment with proton therapy [16].

Tumor site	Proton therapy, %	Gamma-ray therapy, %
Stomach and esophagus	0	11
Colon	0	7
Breast	0	0
Lung	1	7
Thyroid	0	6
Bones and joints	1	2
Leukemia	3	5
All cases of secondary cancer	5	43

* Medulloblastoma is a malignant tumor which is found mainly in children.

The fact that hard radiation damages or kills cells of living organisms has been known since long ago [18]. A cell cytoplasm can tolerate a dose of up to 250 Gy (one gray is equal to 1 J kg^{-1}). The cell nucleus is much more vulnerable than the cytoplasm. A dose from 1 to 2 Gy is sufficient to fatally damage the nucleus because of the destruction of DNA molecules. According to Puck [18], the mechanism of radiation damage of the cell can be described as follows. Irradiation of DNA molecules causes the cells to lose their ability to reproduce. However, cell death does not occur

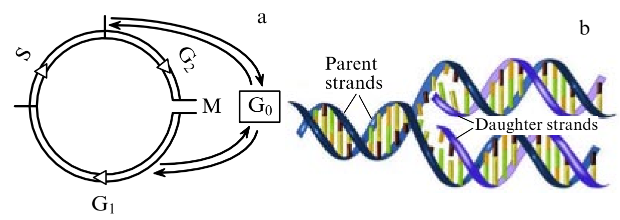

Figure 1. (a) Mitotic cycle of cell development (typical mitotic cycle lasts from 12 to 48 hours): M is mitosis (typical time is about 1–2 hours), G_1 is the resynthetic period, S is the period of DNA synthesis, G_2 is the postsinthetic period, and G_0 is the phase of possible rest. (b) Replication fork dividing the DNA molecule, existing during the mitosis stage.

immediately, because the amount of radiation energy absorbed is negligibly small in comparison with the energy necessary for mechanical disintegration of the cell. Although chromosome functions are broken due to irradiation, the cells remain enzymatically active. The cells continue to play their physiological role until the time comes when they must divide, but they fail.

As is well known, a DNA molecule located in the nucleus of a human cell has the shape of a double helix. Due to various factors, the DNA is prone to damage. Evolution has found a mechanism to repair the molecule when one of the strands appears to be damaged. In the case of a double-strand break, the cell cannot repair the DNA and dies.

A spontaneous break of strands in the DNA molecule occurs during cell replication. In the process of cell division, so-called mitosis (see Fig. 1a illustrating the mitotic cycle of cell evolution), the double helix divides into two single strands, leading to the formation of the 'replication fork' shown in Fig. 1b). The molecular mechanism adds on missing second strands, identical to those in the primary DNA molecule.

In the course of either chemotherapy or radiation therapy, cancer cells are more vulnerable, because they divide more rapidly than healthy cells, and, thus, more often appear in the phase with only one strand. The cell is most vulnerable at the postsynthetic mitosis stage G_2 and during the phase of mitosis (M) (Fig. 1b) [19]. In the M phase, a single-strand molecular fragment appears. Its break leads to irreversible damage to the DNA molecule. Affected in the postsynthetic G_2 stage of mitosis, the DNA molecule has insufficient time to recover. For this reason, less energy is required for the destruction of the DNA molecule in a cancer cell (and the damage probability turns out to be higher) than in a healthy cell. The difference in radiosensitivity of the cancer and healthy cells reaches about 20–25%. Healthy cells appear to be relatively less damaged, and they recover more quickly (often by the factor 2–3) than the cancer cells. In this way, the destruction of malignant tumors happens.

In developed countries, radiation therapy is used to treat up to 70% of cancer patients. The most widely used form is therapy with gamma-rays, where the directed gamma radiation is generated by a beam of relativistic electrons accelerated by a compact linac up to an energy of 25 MeV. The energy of electrons is then converted into the energy of gamma-photons in the course of their interaction with a slab of lead. The resulting beam of so-called bremsstrahlung radiation is directed to the location of a malignant tumor. In the body tissues, the gamma-photons lose their energy due to the photoelectric effect, Compton scattering, and electron–positron pair creation in the electric field of atoms and atomic nuclei. The major part of the energy of the ionizing radiation absorbed by the cells is transferred by a large number of secondary electrons with energies ranging from 1 to 20 eV. Since this energy is on the order of or below the molecular ionization potential, these electrons break one or both of the DNA strands. The basic mechanism of DNA destruction comprises the strand break due to the excitation of resonances within the molecule [20, 21]. Other factors damaging the DNA molecules are associated with the formation of so-called oxidants, i.e., chemically aggressive radicals, in the radiolysis of intracellular water as a result of electron interaction with the tissue molecules. Radicals, in turn, chemically destroy the DNA molecule, resulting in the loss of the cells' ability to replicate. DNA lesions may also occur due to the direct impact of fast ions colliding with atomic nuclei within the molecule and due to DNA ionization by fast electrons [22–24].

We note here the well-known relationship between radiation therapy and space medicine, insofar as one of the main obstacles to interplanetary flights of astronauts and their long-term living on extraterrestrial bases, e.g., on the Moon, is the unacceptably high irradiation from solar and galactic cosmic rays, in view of limited resources for radiation protection under the mission conditions. Here, we see that the methods of estimating radiation doses developed in one area can be applied to solving problems in another area of research [23].

As shown by experiments [20, 21, 25–27], electrons (photons) with an energy of several electron-volts are sufficient for breaking the DNA strands. To deliver the required dose to the location of the tumor, the initial particle energy must be large enough to overcome the energy losses during particle propagation in the tissue. As mentioned above, to fatally damage the DNA molecule in the cell nucleus, the sufficient dose is about 1 Gy. In order to destroy the tumor in the full course of fractionated irradiation (requiring 1 or 1.5 months), the necessary dose ranges approximately 60–70 Gy.

In the above process of secondary electron generation in tissue, a gamma-ray beam with an initial multimegaelectron-volt energy relatively quickly loses its energy. Each elementary act of interaction of gamma photons with electrons takes away almost all the energy of the photon, leading to an exponential decrease in the dose with increasing distance from the surface. The near-surface minimum in the dose distribution with a characteristic size on the order of a few millimeters is associated with the finite distance at which the secondary electrons are produced. This minimum plays a positive role in protecting the skin from unwanted damage, which is an important clinical advantage. However, a significant portion of the gamma-ray beam energy is absorbed in the tissues located in front of and behind the tumor. In this case, the delivery of a high enough dose, conditioned by an acceptably low exposure of the surrounding tissue and organs, can be achieved by using several beams irradiating the malignant tumor from different directions and with different energies.

The utilization of protons (ions) in radiation therapy [28] has a number of advantages over other approaches. This is connected with the following feature of the interaction of protons having an energy of hundreds of MeV with atoms in the tissue. Protons lose energy mainly in collisions with electrons, while the energy transferred to atomic nuclei is a factor of $m_e/(2m_\alpha)$ less and thus negligible. Here, m_e and m_α are the electron and nucleus masses, respectively. Therefore, the protons gradually lose energy during their propagation in the tissue. The energy loss rate is inversely proportional to the square of the particle velocity; therefore, the local dose increases as the ions slow down. This explains the sharp peak (Bragg peak) in the distribution of the delivered dose [29] (see Figs 3 and 4 below). In other words, the distance at which a proton with a certain energy stops is fixed. This circumstance helps to avoid unnecessary irradiation of healthy tissue behind the tumor. The presence of a sharp maximum in the curve of the ion energy losses in matter reflects a substantial increase in the radiation dose in the vicinity of the ion stopping point (see, e.g., Refs [5, 6, 13]). The scattering of the ion beam by the atomic electrons is small, which also reduces the irradiation of healthy tissue surrounding the tumor.

Therapeutic use of proton beams for cancer treatment was proposed by R R Wilson in 1946 [28]. The first patients received radiation therapy in 1950–1960s in the United States (Berkeley and Harvard), in Sweden (Uppsala), and in the USSR (Moscow and Dubna). Since then, about 110 thousand cancer patients have undergone hadron therapy worldwide (90% with the use of protons, and 10% with heavier ions, mainly carbon) [30].

To date, proton beams with the necessary parameters have been obtained with classical accelerators of charged particles (synchrotrons, cyclotrons, linear accelerators). After more than 40 years of experimental research, several clinical centers are being constructed, designed for proton radiation therapy treatment of up to 1000 patients per year. Already 42 such centers operate (for example, the centers of ion radiation therapy in Heidelberg in Germany, Chiba and Harima in Japan, the Paul Scherrer Institute in Switzerland); about the same number are under construction [30]. Unlike research institutes wherein the era of hadron therapy originated, all these centers are equipped with special medical ion accelerators, from which the beams are transported to 3–5 treatment rooms.

A necessary and the most expensive element in such centers is the GANTRY system, which is a device intended for the multifield (from different directions) irradiation of the lying patient. The gantry can rotate the ion beams around the patient, providing tumor irradiation from all needed directions. A gantry for proton therapy has a diameter equal to 12 m, length of 24 m, and weight of 60 tons. The weight of the gantry for a therapeutic treatment by carbon ions is up to 600 tons.

Clinically, the main applications of proton therapy are uveal melanoma (eye tumor) using relatively low-energy particles and, with high-energy protons, various pediatric tumors, chordoma and chondrosarcoma, and cervical and prostate tumors.

Proton therapy (in general, ion or hadron therapy) is believed to have a number of advantages over radiation therapy with gamma-rays because of the lower integral dose received by healthy tissue (especially when modern methods are applied, such as scanning and energy-modulated ion beams), although additional clinical studies are needed for confident assertion. Proton therapy has been used successfully for the treatment of different types of tumors, such as those mentioned above and also large tumors associated with lung cancer, cervical spine tumors, and cervical spinal cord meningiomas.

Heavier ions, such as carbon ions, have additional clinical advantages due to lower scattering effect and greater biological effectiveness in the target compared to X- and gamma-rays and protons. Up to now, carbon ions have been utilized mainly in the treatment of chondroma and chondrosarcoma of the cervical spine, and malignant tumors occurring in salivary glands, the lungs, prostate, liver, and soft tissues [31, 32]. Due to their relatively high electric charge, multiply charged carbon ions passing through matter provide a much denser distribution of ionization events along the particle track than gamma-rays and protons. The distance between the ionization events becomes smaller than the transverse size of the DNA helix. This leads, at the same dosage in terms of energy (Gray), to a larger number of 'irreparable' double strand breaks of the DNA. The number of lethally affected cancer cells dramatically increases. It is the use of ions heavier than protons that is recommended in the case of radioresistant tumors, which amounts to up to 15–20% of the total number of tumors according to various estimates.

The disadvantage of carbon beams is associated with the exposure of the tissue behind the Bragg peak, resulting from nuclear fission projectiles created in the inelastic collisions of heavy ions with atomic nuclei in the body tissue (see below Fig. 3). This disadvantage is almost completely compensated for by making use of multifield (from different directions) irradiation.

A wide implementation of hadron therapy is difficult because it requires an ion accelerator (e.g., a quite large cyclotron or synchrotron) and a system for the ion beam transportation and manipulation. These technically sophisticated elements cost from 100 to 200 million euros in the case of a therapeutic center with four treatment rooms. Consequently, this entails a high cost of medical services. Owing to this difficulty, at present only 42 hadron therapy centers operate around the world, although up to 30% of cancer patients need this form of treatment. Investigations are currently being undertaken in several directions aiming at the development of more compact and less expensive technologies. Several companies are developing compact medical ion accelerators exploiting technologies known in the field of conventional particle accelerators, such as superconducting cyclotrons or compact cyclotrons serving one or a few radiation facilities.

There are other concepts of medical accelerator development. They are associated with synchrocyclotrons, with alternating magnetic field accelerators, and with dielectric wall accelerators [33, 34].

An approach fundamentally different from those mentioned above is based on the idea of a laser ion accelerator [35]. The use of a relatively small-size laser ion accelerator in oncological centers can revolutionize hadron therapy, making high-energy proton and heavier ion beams much more accessible for patients pending treatment.

Articles [35–41] have drawn attention to the fact that the exploitation of a laser accelerator in hadron therapy is very attractive owing to the compactness of such an accelerator and the occurrence of additional options for ion beam parameter control.

One of the main advantages of laser ion acceleration methods over currently designed schemes is that it can simplify and significantly downsize the system for ion transport to the treatment rooms, as well as the facility for the ion beam rotation (gantry). Instead of devices comprising bulky and heavy magnets required for the deflection of ion beams with a high energy (rigidity), it is proposed to use an

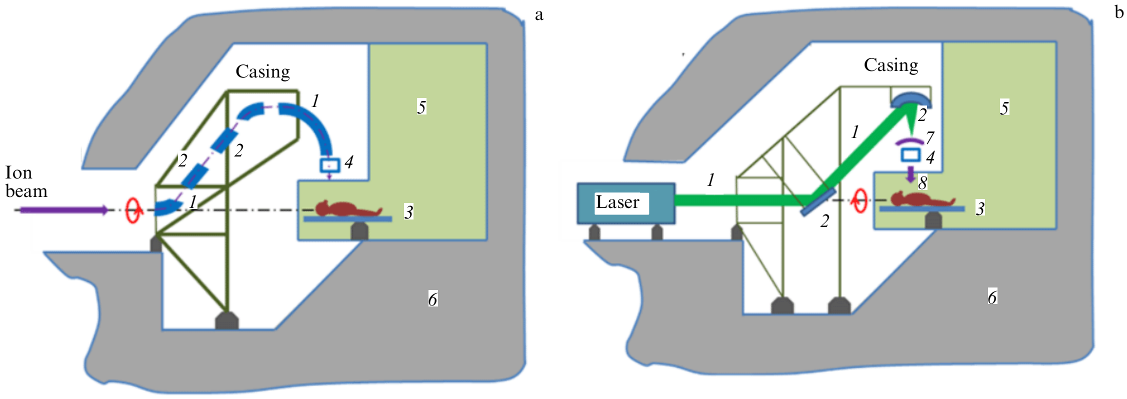

Figure 2. Comparison of the classical setup of a gantry and its optical counterpart [34]. (a) The classical setup of a gantry: (*1*) bending magnets, (*2*) quadrupole lenses, (*3*) positioner, (*4*) system of dose formation and dose monitoring, (*5*) treatment room, and (*6*) concrete protection.(b) Individual laser accelerator and the optical setup of the gantry: (*1*) laser beam, (*2*) optical system of transportation and focusing of the laser pulse, (*3*) positioner, (*4*) dose monitoring system, (*5*) treatment room, (*6*) concrete protection, (*7*) target, and (*8*) ion beam. In both cases, the casing with the elements mounted on it can be rotated $\pm 180°$.

optical system which bends and rotates laser beams, arranging their interaction with a target in such a process that generates fast ions in the treatment room, not outside it.

Various approaches to employing the laser ion accelerator are possible. In the simplest case, the laser particle source is an injector which permits forming an ion beam of high quality with the desired composition. The next one, also a simple option, reduces to replacing the classical accelerator with a laser accelerator, as discussed in Ref. [42]. However, a shortcoming of these approaches is that the above-discussed gantry is not only expensive, but also very bulky (its diameter is 6–8 m, length is 10–12 m) and heavy (100 tons or more). The weight and cost are mostly determined here by the powerful magneto-optical system able to rotate as a whole, which must be fabricated with a high precision. Other setups using laser accelerators seem more attractive. In the most promising approach, laser radiation is directed to a target in a treatment room, where the laser energy is converted into fast ions. This can simplify and make cheaper the classical technical solution in present-day hadron therapy, removing the necessity of a centralized accelerator, a channel (or channels) of ion beam transport, and, finally, of most of the gantry magnetic system.

Figure 2 compares two setups. The classical one for ion beam delivery to the patient and for controling the ion beam parameters (Fig. 2a) is built around magnetic systems. An alternative is one of several possible technical solutions, using an 'optical gantry' with the laser ion accelerator (Fig. 2b). Here, the term 'optical gantry' means an all-optical configuration of the facility for hadron therapy. The advantage of this system over the magnetic one is that it is much easier to direct and bend photon beams with mirrors than to control high-energy ion beams with bulky magnetic optics.

For the implementation of the laser accelerator in hadron therapy, the parameters of accelerated ion beams, in terms of the ion beam energy, stability, and quality, must satisfy the same requirements as established in classical hadron therapy for the ions accelerated by conventional accelerators.

Currently, the energy of ions accelerated in the laser plasma in experiments is approaching the value at which ions can be considered for therapeutic applications. However, some properties of the beam, such as the repetition rate, electric current, energy spectrum, and transverse emittance, have not yet reached the necessary level or are not sufficiently well controllable. For this reason, a prototype of a medical laser accelerator has not yet been built. On the other hand, several world leading scientific centers are involved in investigating physical processes of laser ion acceleration, studying the biological effects of the obtained ion beams, and developing the required technology (e.g., Japan Atomic Energy Agency, Kizugawa [43]; Technical University of Münich, Germany; Institute of Physics of Czech Academy of Sciences, Prague within the framework of the project ELI-Beamlines[1] [44]; University of Catania, Italy [45]; Institute for Heavy Ion Research, Darmstadt, Germany; Rossendorf Research Center, Dresden, Germany; University of Belfast, UK). New methods of treatment planning regarding the peculiar properties of the ion beams generated in laser plasma are also under development [46]. Crucially important results of these studies have been achieved in experiments on cancer cell irradiation by beams of protons accelerated with laser radiation [47–54]. Further progress in this scientific area is associated with the demonstration of more efficient and better controlled ion acceleration mechanisms, with the use of tailored targets, and, importantly, with the development of laser technology enabling generation of powerful and stable high-quality pulses of electromagnetic radiation.

The development of laser ion accelerators for hadron therapy has already been criticized at the initial stage in Refs [13, 55]. Some publications criticise not only the proposed usage of laser ion accelerators but all radiation therapy [56] (see reply in Ref. [57]). This reflects a high level of competition in modern medicine. One of a few obvious reasons for the critical attitude towards laser accelerators is that the authors of Refs [13, 55] lack awareness of the mechanisms of ion acceleration in the light field of high-power lasers, methods for high-quality ion beam generation, and the experimental results obtained in this area. In order to show that our assessment is not unfounded, we note that in the review paper [13] the mechanism of ion acceleration is assumed to be based on acceleration by wake plasma waves, with a reference to an experiment on the acceleration of electrons, not ions (sic!). One of the main conclusions reported in Ref. [55] is that the experts in the field of laser

[1] ELI — Extreme Light Infrastructure.

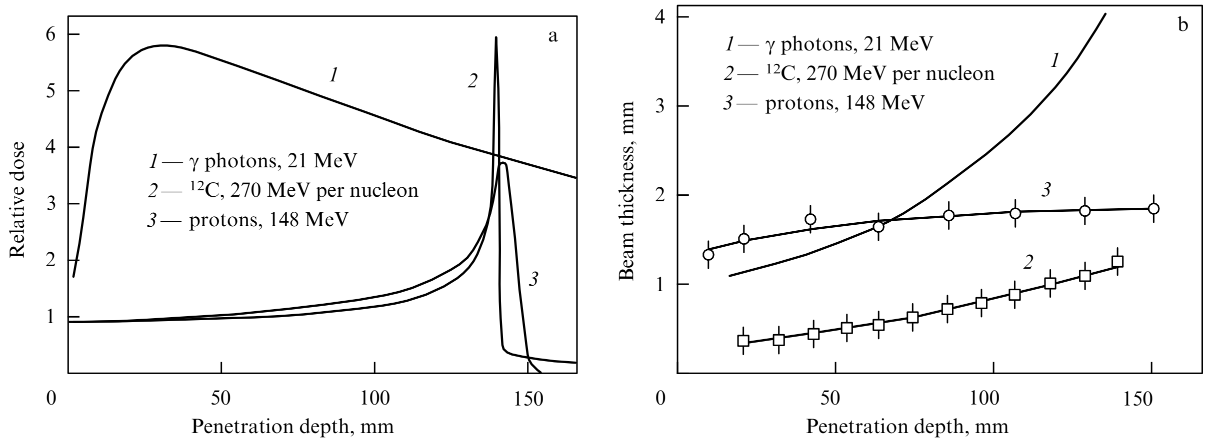

Figure 3. (a) Measured dose as a function of penetration depth for protons, carbon ions, and gamma-rays. (b) Scattering of ion and photon beams in the transverse direction, characterized by the growth of the cross section (thickness of the beam), for the same values of the penetration depth [69–71] (see also Ref. [43]).

acceleration are not aware of methods for ion beam quality improvement, despite the fact that one such method was proposed in 2002 in Ref. [35] devoted precisely to laser-accelerated ion beam quality perfection, then demonstrated using both numerical simulations [38, 58, 59] and experiment [60].

The above-mentioned critical attitude may be in part caused by a lack of review papers summarizing recent findings, although the relationship between the studies of laser methods of ion acceleration and the problems of hadron therapy has been noted in reviews [61–68] devoted to the general problem of charged particle acceleration in laser plasmas. The present review article attempts to fill this gap.

2. Hadron therapy using ion beams accelerated with classical accelerators

2.1 Physical and biological characteristics

The main reason why ion beams are preferable to bremsstrahlung gamma-ray beams for the irradiation of malignant tumors is that the radiation dose grows with the depth of ion beam penetration, acquiring a sharp maximum at the beam stopping point, called the Bragg peak. At the entrance of the beam, where the ion energy is maximum, the production cross section of electrons and atomic nucleus fragments (due to collisions of fast ions with the target atoms) is small, and the radiation dose is correspondingly small. The most intensive creation of particles produced in collisions of fast ions with atoms occurs at the end of the ion trajectory in the vicinity of the Bragg peak, where the ions have a relatively low energy of about 10–20 MeV per nucleon, but still remain fully ionized. On this portion of the ion trajectory, the time of ion interaction with the medium increases due to a decrease in the ion velocity. This leads to the ionization growth in the medium caused by atomic collisions with ions and due to the formation of a channel with a large concentration of free electrons. This gives rise to a relatively large local radiation dose in this zone (Fig. 3a). This behavior is typical for all kinds of ions. In the case of heavy ions interacting with the target, the density of ionization events can be substantially higher, so that the distance between them becomes smaller than the lateral size of the DNA helix. This causes an 'unrepairable' double strand break in a large number of DNA molecules. Due to the Bragg peak, the relative biological effectiveness (RBE) increases by a factor of 3 to 5 compared to its value at the entrance (on the initial portion of the ion trajectory).

The RBE, by definition, is equal to the ratio of the dose D_γ brought by X-rays or gamma-rays to the dose D_α brought by the α ions, which is required to achieve the similar biological effect:

$$\mathrm{RBE} = \frac{D_\gamma}{D_\alpha} \,. \tag{1}$$

The dose given by an artificial source of photons $^{60}\mathrm{Co}$ is adopted ($\mathrm{RBE} = 1$) as a reference for D_γ.

The percentage of cells that survive the exposure with the dose D is approximated by the expression

$$S(D) = \exp\left(-\alpha D - \beta D^2\right) \tag{2}$$

with the coefficients α and β. The ratio α/β is a measure of the radiosensitivity of tissues (see Ref. [13]).

In clinical applications, carbon ions have a biological effectiveness by a factor of 2 to 3 higher than protons, while the RBE at the entrance is relatively low. Moreover, carbon ions with the same energy and, correspondingly, the same linear energy transfer (LET)[2] have different RBEs for various kinds of cells. The RBE is higher for radioresistant self-repairable cells and lower for nonradioresistant cells, including benign cells [69]. Thus, carbon ions have high values of RBE where it is necessary (at the end of the trajectory, at the location of the irradiated tumor), and just for those cells (radioresistant) which must be destroyed. These properties enable successful irradiation of radioresistant tumors with carbon ions and are the main motivation for a carbon ion use in hadron therapy [13, 70].

For clinical applications, the ion beam parameters are chosen with respect to the geometry of the tumor. These parameters are the beam size in the longitudinal and transverse directions and the size of the region of maximum

[2] LET is the energy transferred to a medium by an ionizing particle per unit length along the particle trajectory.

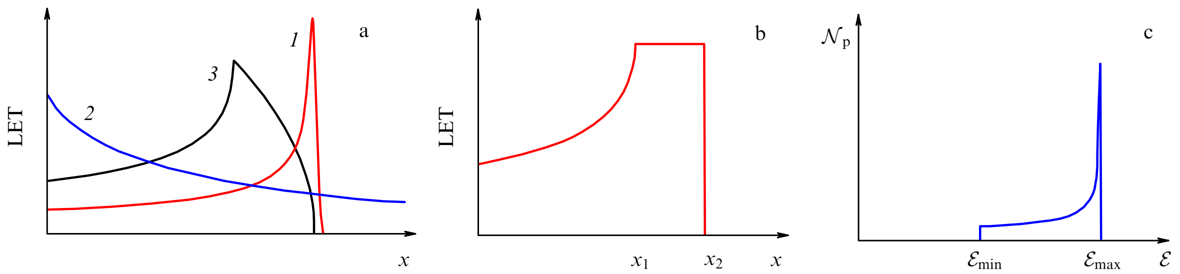

Figure 4. (a) Amount of energy delivered into the matter per unit length along the trajectory of a fast proton beam (linear energy transfer, LET) with different energy spectra: (*1*) monochromatic beam, $n_0\delta(\mathcal{E}-\mathcal{E}_{\max})$, (*2*) quasithermal beam, $n_0\theta(\mathcal{E}_{\max}-\mathcal{E})\exp(-\mathcal{E}/T)$, and (*3*) beam with a piecewise constant energy spectrum, $n_0\theta(\mathcal{E}-\mathcal{E}_{\min})\theta(\mathcal{E}_{\max}-\mathcal{E})$. (b) Profile of the energy transferred by the beam (LET) with the energy spectrum in figure (c), described by expression (13).

energy release in the longitudinal direction, determining the shape of the dose distribution. A finite width of the ion energy spectrum leads to the broadening of the Bragg peak and to its transformation into a plateau. The stochastic nature of ion scattering in a medium also causes Bragg peak broadening (see review article [13] and literature cited therein). The lateral size of the beam also increases, resulting in the irradiation of healthy tissues at the lateral margins of the tumor. This effect is stronger for proton beams [71] than for beams of heavier ions, such as carbon ions (Fig. 3b), so that the employment of heavier ions provides a better irradiation scenario. All the above advantages of ions heavier than protons give grounds for a conclusion that laser accelerators should be considered as a tool for the generation of not only protons, but also heavier ions.

2.2 Energy losses and ion beam scattering

Here, we discuss the mechanism of ion energy loss in matter in more detail. As is known [72] (see also Refs [12, 73]), an ion beam propagating in matter loses its energy at the rate

$$\frac{d\mathcal{E}}{dx} = -F(\mathcal{E})\,, \tag{3}$$

given by the expression

$$F(\mathcal{E}) = \frac{\eta}{\mathcal{E}}\,\Lambda(\mathcal{E})\,, \tag{4}$$

where $\Lambda(\mathcal{E})$ is a function of the ion energy $\mathcal{E}$; its particular form depends on the state of matter. According to Ref. [74], the coefficient η is equal to

$$\eta = \frac{4\pi e^4 m_\alpha Z_{\rm u} Z_\alpha^2}{m_{\rm e}}\,, \tag{5}$$

where for the function $\Lambda(\mathcal{E})$ we have

$$\Lambda(\mathcal{E}) = \ln\frac{2m_{\rm e}\mathcal{E}}{m_\alpha\langle I_{\rm ioniz}\rangle} - \ln(1-\beta^2) - \beta^2 - \frac{C}{Z_{\rm u}} - \frac{\delta}{2}\,. \tag{6}$$

Here, $Z_{\rm u}$ and Z_α are the charges of the nucleus and of the fast ion, respectively. The normalized velocity of a proton with an energy on the order of 200 MeV or a carbon ion with 400 MeV per nucleon is approximately equal to $\beta \approx 0.7$. The mean ionization potential $\langle I_{\rm ioniz}\rangle$ for water reaches 79.7 eV. The last two terms on the right-hand side of Eqn (6) describe the effects of the finite density of the medium and the atomic shell effects.

The dose delivered by an ion beam with luminosity w, which is equal to the number of particles per cm^2, to a target with the density ρ is given by

$$D[\text{Gy}] = 1.6\times10^{-9}\times\frac{d\mathcal{E}}{dx}\,[\text{keV}\ \mu\text{m}^{-1}]\ w\,[\text{cm}^{-2}]\ \rho\,[\text{g cm}^{-3}]\,. \tag{7}$$

As an example, we consider the case of fast protons. The dependence of the particle distribution function $\mathcal{N}_{\rm p}(x,\mathcal{E})$ on the coordinate and energy is described by the transport equation

$$\frac{\partial\mathcal{N}_{\rm p}}{\partial x} + \frac{\partial}{\partial\mathcal{E}}\big(F(\mathcal{E})\mathcal{N}_{\rm p}\big) = 0 \tag{8}$$

with the boundary condition $\mathcal{N}_{\rm p}(x=0,\mathcal{E}) = \mathcal{N}_{\rm p,0}(\mathcal{E})$. The solution of Eqn (8) can be written in the form

$$\mathcal{N}_{\rm p}(x,\mathcal{E}) = \mathcal{N}_{\rm p,0}(\mathcal{E}_0)\left|\frac{d\mathcal{E}_0}{d\mathcal{E}}\right|, \tag{9}$$

where the current $\mathcal{E}$ and initial $\mathcal{E}_0$ particle energies are related to the particle coordinate x through the expression

$$\int_{\mathcal{E}_0}^{\mathcal{E}}\frac{d\mathcal{E}}{F(\mathcal{E})} = -x\,. \tag{10}$$

Using Eqns (3), (9), and (10), we find the energy loss rate of the beam or, equivalently, the value of the linear energy transfer:

$$\text{LET}(x) = \int\mathcal{N}_{\rm p}(x,\mathcal{E})\,F(\mathcal{E})\,d\mathcal{E}\,. \tag{11}$$

Figure 4a depicts the dependence of the energy transferred by beams of fast protons with different energy spectra at $x = 0$. Curve *2* corresponds to a beam with a quasithermal energy distribution:

$$\mathcal{N}_{\rm p}(x=0,\mathcal{E}) = n_0\theta(\mathcal{E}_{\max}-\mathcal{E})\exp\left(-\frac{\mathcal{E}}{T}\right). \tag{12}$$

Here, $\theta(\xi)$ is the unit step Heaviside function, $\theta(\xi)=1$ for $\xi>0$ and $\theta(\xi)=0$ for $\xi<0$. A quasithermal distribution function of fast protons corresponds to the dependence which typically approximates the energy spectra of fast protons obtained in experiments on the interaction of laser radiation with solid targets and in numerical simulations with non-optimal targets. The maximum energy of accelerated particles

$\mathcal{E}_{\max}$ is several times larger than the effective temperature T of the beam. We see that a quasithermal beam loses its energy mainly at the entrance of the irradiated target.

The dependence of the rate of energy loss on the coordinate for the quasithermal beam is obviously unsuitable for the purposes of hadron therapy. For a monoenergetic ion beam, whose particle energy distribution has the form $\mathcal{N}_{\mathrm{p}}(x=0,\mathcal{E}) = n_0\delta(\mathcal{E}-\mathcal{E}_{\max})$, the dependence of the energy transferred into the medium per unit length on the coordinate (curve *1* in Fig. 4a) has a pronounced maximum, the Bragg peak.

Neglecting the logarithmic dependence of the losses on the energy in formula (10), we can solve analytically integral equation (11) with respect to the desired distribution function $\mathcal{N}_{\mathrm{p},0}(\mathcal{E})$ for a given distribution $\mathrm{LET}(x)$, since equation (11) in this approximation is reduced to the well-known Abel integral equation. For example, a uniform energy deposition within the interval $x_1 < x < x_2$ is provided by the ion beam with a spectrum

$$\mathcal{N}_{\mathrm{p}}(x=0,\mathcal{E}) = n_0\,\frac{\theta(\mathcal{E}-\mathcal{E}_{\min})\,\theta(\mathcal{E}_{\max}-\mathcal{E})}{\sqrt{\mathcal{E}_{\max}^2-\mathcal{E}^2}}\,, \qquad (13)$$

where the maximum and minimum energies, $\mathcal{E}_{\max}$ and $\mathcal{E}_{\min}$, are related to the coordinates x_1 and x_2 of the irradiated region by formulas $\mathcal{E}_{\max} = \sqrt{\eta x_2}$ and $\mathcal{E}_{\min} = \sqrt{\eta x_1}$, respectively. Figure 4b shows the profile of the energy deposited by the proton beam with a given energy spectrum. Such a spectrum can be prepared by tailoring in a special way the proton distribution inside the target (see discussion below), or it can be formed by a superposition of several monoenergetic beams.

Using relationship (10) between the initial ion energy and the distance at which the ion loses all its energy, we can find the expression for the energy of a heavy α-ion penetrating at the same depth as a proton with the energy $\mathcal{E}_{\mathrm{p}}$:

$$\frac{\mathcal{E}_\alpha}{A_\alpha} = \mathcal{E}_{\mathrm{p}}\,\frac{Z_\alpha}{\sqrt{A_\alpha}}\,. \qquad (14)$$

Here, A_α is the atomic mass of the heavy ion. For example, referring to the case of a proton with the energy $\mathcal{E}_{\mathrm{p}} = 200$ MeV, for helium ions we obtain $\mathcal{E}_{\mathrm{He}}/A_{\mathrm{He}} = 200$ MeV/n, and for carbon C^{+6} ions we obtain $\mathcal{E}_{\mathrm{C}}/A_{\mathrm{C}} \approx 400$ MeV/n.

As noted above in Section 2.1, the scattering of the beam by the atoms of the medium results in the beam broadening in the transverse direction. According to Ref. [75], the angular dispersion of particles is proportional to the square root of the particle path length and is inversely proportional to the particle energy. The typical lateral size of therapeutic beams inside water is on the order of several millimeters.

If there are radiation-sensitive organs close to the beam axis, then it is desirable to use an ion beam with a high enough energy, for which the angular dispersion is acceptably small. Then the cost of such a choice is the loss of the advantage of possessing the Bragg peak [33] and the necessity of involving a large number of ion beams irradiating the tumor from different angles.

In the course of heavy ion interaction with atomic nuclei of the medium, radioactive isotopes are also produced (induced radioactivity of the medium). In the process of these isotopes decaying, positrons are emitted, which are used to monitor the dose, delivered by fast ions [76–78], with the help of positron emission tomography (PET).

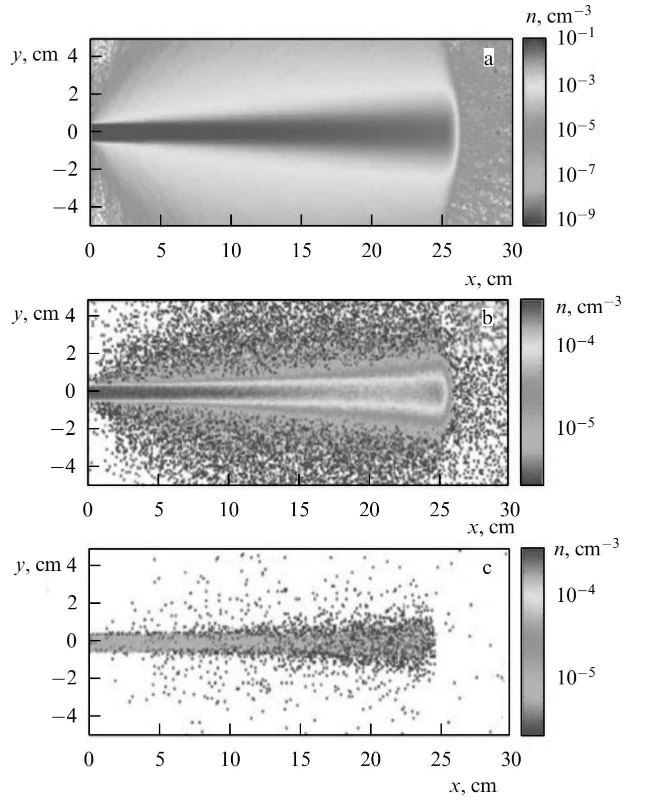

Figure 5. Simulated results of nucleus radioactivation by a proton beam during water layer irradiation (the target boundary is at a distance of 5 cm from the left border of the computational domain) [43]. The diameter of a 200-MeV ion beam at the entrance to the target is equal to 10 mm. Grey scale specifies the particle density n. (a) Spatial distribution of particles in the proton beam. (b) Distribution of nuclei of the oxygen ^{15}O isotope. (c) Distribution of nuclei of the carbon ^{11}C isotope.

The exploitation of particle injectors with a complex ion composition opens up additional opportunities for the implementation of efficient scenarios of tumor irradiation, as well as for diagnostic purposes. From the results of computer simulations [79] and experiments [80] on the interaction of powerful laser radiation with thin solid-density foil targets comprising light and heavy ions, it follows that there emerges the possibility of obtaining beams of fast fully ionized ions. If a proton beam irradiating tissue has a small number of carbon and/or oxygen ions, nuclear reactions induced in the tissue by those heavy ions generate radioactive isotopes. As noted above, it is possible to control the delivered dose distribution in real time by using positrons emitted by unstable carbon and oxygen isotopes.

For monitoring the dose with nanosecond time resolution, gamma-rays emitted in nuclear transitions induced by protons can be useful, since the gamma-ray spectrum corresponds to the proton energy [81, 82]. It should be noted that dose monitoring is also carried out using methods based on nuclear magnetic resonance (see review articles [83] and [84] devoted to a discussion of the methods of dose verification *in vivo* in proton therapy and in NMR tomography).

Figure 5 presents the simulated results of the water radioactivation by proton beam irradiation [43]. A computer code developed in Ref. [85] and based on the Monte Carlo method was applied. The boundary of the water layer target is localized at a distance of 5 cm from the left boundary of the computational domain. The diameter of a proton beam with the energy of 200 MeV at the entrance is 10 mm. The spatial distribution of the particles in the proton beam is plotted in Fig. 5a. It is seen that, due to beam spreading, its lateral size increases. As a result of inelastic proton collisions with atomic nuclei, the oxygen ^{15}O and carbon ^{11}C isotopes are created. Their spatial distributions are shown in Figs 5b and 5c.

2.3 Scenario of passive irradiation of a target: methods for ion beam broadening

In order to ensure positive treatment results, it is crucial to adjust the beam energy deposition region to the malignant tumor (target). Ion beams generated by accelerators are characterized by a narrow energy spectrum and by a low divergence angle (i.e., a small transverse emittance), which corresponds to a beam lateral size of about a few millimeters. These parameters are determined by the beam acceleration and transportation requirements. However, the size of the beam must be increased both in the transverse and in the longitudinal directions when irradiating a sufficiently large target with a volume on the order of or greater than 100 cm^3.

Currently, the majority of hadron therapy centers apply the methods of passive beam broadening, similar to those developed in radiology manipulating with X-ray beams. Schematic of the corresponding instrumentation for controling the ion beam parameters is shown in Fig. 6a. The original monoenergetic sharply collimated beam is broadened in the transverse direction by a diffuser (a foil with a certain thickness) which makes the distribution of particles uniform over a larger diameter. Then, passing through holes whose shape corresponds to the shape of the tumor, the beam takes the form adjusted to the target. After that the beam particles pass through thickness-modulated decelerating filters. Since the energy loss is proportional to the thickness of the filter, different parts of the beam lose different energies. In this way, the beam energy spectrum is modified. In the case of a proton beam, the energy spectrum should ensure the formation of a plateau in the LET curve with the length equal to that of the target.

For carbon ions, one has to form some curve, not a plateau. The product of this curve and the RBE determined at each cross section in depth must give the same biological dose, not the same absorbed dose (in energy terms). The planned spatial distribution of the dose determines the shape of the filters modulating the ion beam energy. In this way, the parameters of each filter must be set in accordance with the desired distribution of the RBE within a particular target. An overview of the methods of passive ion beam broadening is given by Chu et al. [5].

2.4 Scenario of active target irradiation

The scenario of active target irradiation is based on employing the transverse deflection of ions by a magnetic field [86]. It was first implemented for proton beams at the Paul Scherrer Institute (PSI) in Villingen (Switzerland) [87] and, in the case of carbon ions, at the Institute for Heavy Ion Research (GSI) in Darmstadt (Germany) [88].

The principle of active irradiation of a tumor is illustrated in Fig. 6b. The volume of the target is divided into a sequence of layers that are localized at the same depth. In other words, the tumor is represented as a set of layers, which can be reached by particles having the same energy. Using two fast-

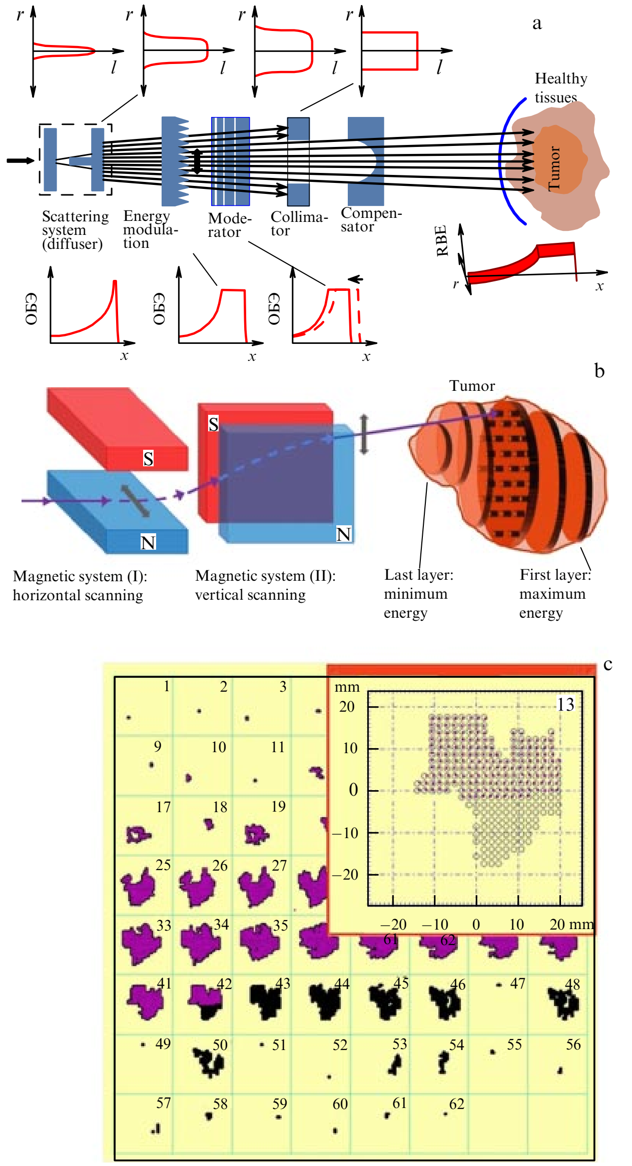

Figure 6. (a) Schematics of a passive formation of the dose field [5]. For the formation of a radially uniform beam source, the original ion beam is widened in the transverse direction in the scattering process in a system of thin foils. The modulation of the beam energy leads to the depth-modulated particle penetration. The moderator shifts the spectrum towards small energies, thus changing the relative biological effectiveness. The collimator restricts the lateral size of the beam in accordance with the target shape. The compensator serves to specify the dependence of the penetration depth of the particles on the transverse coordinates. (b) Active target scanning [8]. The volume of the target is represented as a set of layers located at the same depth, with each layer consisting of separate sequentially irradiated voxels. (c) Set of images of the layer with different energy depths in the irradiated target volume [86] (see also Refs [13, 44]).

varying magnets deflecting sharply collimated ion beam in the vertical and horizontal directions, the target is scanned voxel-by-voxel, starting with the outermost layer.[3] Upon completing the scan of a layer, the beam energy is set smaller, and the next layer is scanned. Each of the layers is covered with a grid of separate sequentially irradiated voxels.

[3] A voxel is a volume element in the discrete representation. Voxels are the three-dimensional analogues of two-dimensional pixels.

There may be scenarios where the beam is delivered to separate 'spots' (voxels) which minimally overlap along the raster, or the irradiation is sent to almost continuously overlapping voxels. The first approach was implemented at the Paul Scherrer Institute in Villingen [87], while the second has been realized at the Institute for Heavy Ion Research in Darmstadt [88].

In the process of irradiation, the beam intensity is measured every 100 μs. The dose delivered to each voxel is controlled with monitors installed near the patient. Although the layers usually have quite complicated contours, within the scenario of active irradiation the target volume can be 'filled' with a high accuracy.

Figure 6c demonstrates a complete set of images of isoenergy layers obtained during patient treatment. In the inset (with a higher resolution) to the upper-right part of Fig. 6, the circles represent the expected area in which the particles are focused, with the superimposed image of the measured ion beam center position. The beam diameter slightly exceeds the size of each circle, which leads to some overlap of the irradiated areas, thus providing dose uniformity across each of the layers. By gradually changing the beam energy, layer coupling can also be achieved in the longitudinal direction, taking into account the unequal densities of different layers. Controling the characteristics of a proton beam allows the attending physician to devise a tumor irradiation plan in each particular case.

Since cyclotrons produce ion beams with a fixed energy, the desired value of the beam energy is achieved using passive ridge filters modulating the energy spectrum, after which the beam is 'cleaned' by removing ions with too high and/or low energy. The spectrometer is practically placed in the path of the beam, where a magnet deflects the particles with various energies through different angles. From the obtained particle 'fan', a movable collimator selects the monoenergetic beam of particles of the desired energy. As a result, over 95% of the particles from the original beam are lost, leading to an undesired consequence: a large number of neutrons are generated when these 95% of the particles are stopped in the collimator.

When synchrotrons are exploited, the energy of accelerated particles can be selected immediately after their ejection. The required energy values are specified in each acceleration cycle. In addition, in order to reduce the time of scanning, it is required to choose the optimal intensity of the beam in each cycle of acceleration. In practice, for a typical target volume of 100 cm^3, from 30 to 60 isoenergy layers contain from 30 to 50 thousand voxels, which can be irradiated by the particle beam for 3–5 min. The results obtained at the National Institute of Radiological Studies in Japan (NIRS, Japan) promise to reduce the total exposure time to 20 s, largely due to improved control of the data gathered by monitors in a region in front of the patient. In the future, by using beams with varying energy accelerated by synchrotrons, it seems that it will be possible to complete therapeutic irradiation of a tumor in less than 5 s. Reducing the time of exposure is very important for correct alignment of the dose distribution in the target, which alters its position and shape, for example, due to breathing. Practising the standard trick of holding one's breath for a few seconds, it will become possible to irradiate such tumors with the same accuracy as fixed targets, for example, intracranial ones [89].

3. Requirements for a therapeutic system using a laser ion accelerator

Acceleration of charged particles in laser plasmas occurs under conditions significantly different from those typical of the process of particle acceleration in conventional accelerators. Instead of trying to reproduce in the laser plasma the temporal and energy characteristics of the ion beam as in conventional accelerators, unavoidably using obviously undesirable magnetic systems of transportation, including gantries, it is necessary to formulate and implement a novel strategy of particle beam delivery and target irradiation, which will enable full-scale usage of the advantages inherent in laser methods of acceleration.

At present, there is a well-developed theory of ion acceleration in the interaction of powerful laser radiation with matter, whose review can be found in papers [61–68, 90]. As for experimental results, thus far the broad energy spectra of ions have been typically (without using profiled targets) observed, with a maximum energy close to 100 MeV per nucleon for carbon ions [91–94], and up to 160 MeV for protons [95]. Although the total number of particles accelerated during the period of one laser pulse is large enough, the repetition rate at which the subsequent bunches are generated is limited by the maximum repetition rate of the laser. For lasers with a pulse duration in the femtosecond range, the repetition rate reaches the level of several pulses per second. Under conditions typical for the majority of experiments, when the acceleration of the ions occurs in the electric field induced during charge separation in the layer at the target rear surface, the maximum energy of ions is determined by the laser radiation intensity [96]. In the limit of strong violation of the plasma electroneutrality, the energy of fast ions is proportional to the square root of the laser power for relatively long laser pulses with a duration of ≈ 150 fs (see Fig. 9 in Ref. [61]). Such a dependence of the fast ion energy on the laser energy (and on the power for focal spot sizes of the same order) can be seen in Fig. 7a. Extrapolation of this dependence to the region of energies that will be achieved by next generation petawatt lasers and taking account of theory and simulation results allows us to predict the possibility of generating protons with an energy of about 200 MeV required for radiation therapy in the nearest future [5, 6, 97]. Notice that other acceleration mechanisms, such as ion acceleration by the radiation pressure of light [98–102] and the effects caused by a strong quasistatic magnetic field in the near-critical density plasma (see Refs [103–108] and discussions in Sections 4.3 and 4.6), can provide even higher particle energies.

Table 2 summarizes typical magnitudes of the ion beam parameters required for hadron therapy [7, 109]. The beam parameters essentially depend on whether the chosen method of a target irradiation is passive or active. In all cases, however, the maximum energy should be equal to 250 MeV/n for protons, and to 430 MeV/n in the case of carbon ions. To provide a dose of 4 Gy, necessary for the irradiation of 250 cm^3 targets, the proton beam intensity must be equal to 5×10^{10} s^{-1}, and to 10^9 s^{-1} for carbon ions. The required ion beam repetition rate, the beam intensity and the dynamic range of changing the particle number in a beam pulse also depend on the chosen irradiation method. In passive systems, the acceptable repetition rate of changing the delivered dose is about 0.1 Hz, with the dynamic range of changing particle number per pulse equal to 10. The acceptable energy

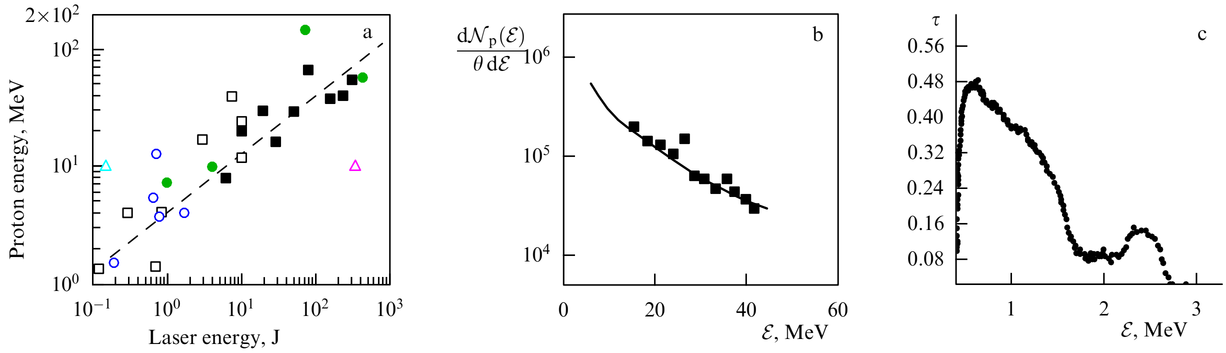

Figure 7. (a) Compilation of data showing the dependence of the maximum energy of ions (protons or energy per nucleon) achieved in experiments with different lasers on the laser pulse energy [64, 91–95]. The dashed line corresponds to the dependence $\mathcal{E}_{las} \propto \sqrt{\mathcal{E}}$. (b) Dependence of the number of accelerated protons in MeV per steradian on energy in MeV obtained in experiment [91] as a result of irradiation of 0.8-μm thick aluminum foil by a femtosecond laser pulse with a power of 200 TW. (c) Energy spectrum of protons observed in Ref. [65]. The ordinate is the optical thickness of the X-ray film.

Table. 2. Ion beam parameters required for hadron therapy in the passive scenario of target irradiation (Passive Dose Delivery Scheme — PDDS) and active irradiation scenario (Active Dose Delivery Scheme — ADDS).

Parameter	Unit of measure	Value
Maximum energy Protons Carbon ions	 MeV MeV per nucleon	 250 430
Intensity (the maximum number of particles per second): Protons Carbon ions	s^{-1}	 5×10^{10} 10^9
Width of energy spectrum	$\Delta\mathcal{E}/\mathcal{E}$	10^{-2}
Discrete step of beam energy control	MeV	5
Bunch duration*	ms	400 – 1000
Repetition rate	Hz	0.15 (PDDS) 20 (ADDS)
Dynamic range of control of the particle number per bunch		10 (PDDS) 10^3 (ADDS)

* As for the bunch duration, it is desirable but, apparently, hardly achievable in laser plasma accelerating ion beams.

spectrum width of the ion beam is about 1–2%, because in order to form the desired beam profile the energy moderators and degraders are used. However, since within the framework of the passive dose delivery scheme the beam–target matching is poorer than the matching typical for X-ray radiation, this leads to undesirable irradiation of healthy tissues outside the tumor. For this reason, therapeutic units coming into operation are equipped with scanning systems for implementing an active scenario of target irradiation.

If the active dose delivering scheme is utilized, the situation becomes quite complicated. In general, the required ion beams should have a spread in energy equal to 1%, with the energy change controllable with a step of less than 5 MeV. The repetition rate depends on the beam duration. It is hard to expect that ion beams with a pulse duration of no less than 1 to 10 s will be achievable with a laser accelerator, because the typical duration of the beam from laser accelerators falls in the range from several picoseconds to nanoseconds. Long beams would allow the irradiation of a large number of voxels with one beam. In this case, it would be sufficient to have the laser repetition rate equal to 1 Hz. In the other limit, when one voxel is irradiated by one bunch, the required repetition rate is on the order of kHz, which is extremely difficult to obtain with present-day laser accelerators. In any case, the number of particles delivered to one voxel should be controlled with an accuracy of not less than 3%, with a dynamic range of the particle number variations from one to two orders of magnitude, which in turn assumes the availability of appropriate monitors placed in front of a patient.

Within the framework of the concept formulated in Ref. [35], the implementation of laser methods of ion acceleration in hadron therapy can help to avoid the use of magnetic systems during acceleration, transport, and manipulation of high-energy ion beams, or it may restrict the use of magnetic systems in a minimum option. Instead of magnetic systems, it was proposed to utilize the all-optical system, sometimes referred to as the 'optical gantry', in which the laser radiation is transmitted to a treatment room, where it accelerates the ions in close proximity to the patient in the desired direction. With the targets tailored in a special way, it becomes possible to provide not only the desired energy of ions, but also their energy spectrum, the longitudinal and transverse emittances and directivity.

In the present article, following widely accepted terminology, we use the word 'target' in one case to denote tumors irradiated by an ion beam, and in another case, a layer of plasma, gas jets, clusters, thin metal or plastic foil, in the process of interaction with which the laser accelerates the ions. However, this should not lead to ambiguity, as this terminology is used in different contexts in different sections of the article.

Targets designed for fast ion generation with a special form and orientation relative to the direction of propagation of the laser beam can be tapped for scanning and focusing the ion beam on the desired area. At the same time, sufficiently fast control of the ion beam intensity and position is needed to provide the required distribution and matching of the delivered dose.

Since the active dose delivery mechanism with scanning requires a high-repetition-rate laser ion accelerator, it is desirable to formulate different approaches and irradiation scenarios. For example, to reduce the required number of pulses and, accordingly, the laser repetition rate, the tumor volume can be subdivided into a set of separate columns instead of the above-mentioned voxels. Each column is irradiated by a single ion bunch with a specially prepared energy spectrum, in which the values of the maximum and minimum energies are controlled. Particle beams with such spectra can be obtained by invoking the methods described above (see Section 2.3) or/and by invoking tailored laser targets, as discussed below in Sections 4.1 and 4.2. Simple estimates show that the required number of laser pulses thus considerably decreases: instead of approximately 10,000 voxels, it is enough to irradiate less than hundreds of columns [110].

4. Mechanisms of ion acceleration in laser plasmas

The fact that ions can be generated in the process of interaction of laser radiation with various targets was established experimentally in the early 1960s. Under the conditions of the experiments at that time, the ion source comprised the plasma formed on the surface of relatively large targets heated by the laser radiation. Beams of fast ions were directed towards the laser pulse. Laser power growth, the transition to shorter pulses, and the increase in the radiation contrast have led to the realization of processes where the ions are accelerated in the direction of the laser radiation propagation. Their source was localized at the rear side of the target with respect to the laser beam. Some of the first theoretical work predicting such a mode of acceleration is reported in Refs [111–115].

At present, the maximum energies of ions accelerated by femtosecond lasers interacting with thin solid targets are 40 MeV [91], 45 MeV [92], and 80 MeV [93] for protons (see also paper [95] announcing the 160 MeV energy) and 1 GeV, i.e., 83 MeV per nucleon in the case of carbon ions [94].

As the theory of charged particle acceleration by an intense electromagnetic radiation predicts, it is possible to obtain with the usage of existing and/or planned lasers the ion beams with energies in the range of a few hundred MeV, which corresponds to the requirements of hadron therapy. The choice of lasers able to generate femtosecond pulses is preferable. This conclusion follows from the steeper dependence of the ion energy on the laser radiation intensity in the case of ultrashort pulses than with the long pulse lasers. In addition, the important fact that femtosecond lasers are more compact and have a higher repetition rate should also be noted.

Unlike laser electron acceleration, based predominantly on acceleration by plasma wake waves in low-density plasma [116], the high-energy ions can be generated by different mechanisms (see, e.g., Refs [43, 117–123]). Below, we shall address those ion acceleration mechanisms which are of high importance for applications in hadron therapy.

The simplest mechanism of acceleration is based on the fact that an electromagnetic wave with a sufficiently large amplitude can accelerate charged particles in a vacuum to the desired energy. In a planar electromagnetic wave, a particle with the charge $Z_\alpha e$ and mass $m_\alpha = A_\alpha m_{\mathrm{p}}$ acquires the energy [124]

$$\mathcal{E}_\alpha = m_\alpha c^2 \left[1 + \left(\frac{Z_\alpha m_{\mathrm{e}}}{m_\alpha} \right)^2 \frac{a^2}{2} \right], \qquad (15)$$

where the normalized wave amplitude is given by $a = eE/m_{\mathrm{e}}\omega c$. Ion acceleration by an electromagnetic wave in a vacuum for the purposes of hadron therapy has been considered in Refs [125–128]. In order to accelerate a proton to the desired energy of 200 MeV by a sharply focused electromagnetic pulse, the required power of the laser radiation must be on the order of one petawatt [126–128]. To accelerate fully ionized carbon ions to 400-MeV/nucleon energy, the radiation power should be equal to 8 PW, which imposes too high a requirement on laser systems. For this reason, most attention in the theory and experiment is paid now to collective methods of ion acceleration, because a long-lived static or low-frequency collective electromagnetic field can be produced in the process of interaction of electromagnetic waves with plasma, which may accelerate charged particles to energies significantly greater than the value given by expression (15).

The idea of laser ion accelerators is based on the high efficiency of laser energy conversion into the energy of fast ions in the process of radiation interaction with plasma in the limit when the laser power reaches the petawatt level. Collimated beams of fast ions are recorded in experiments on the interaction of laser pulses with solid and gas targets [61–68]. The number of particles in the beam and the conversion efficiency of laser energy into the energy of fast ions can reach 10^{13} and 10%, respectively.

Investigations of the processes of ion acceleration rely heavily on the computer simulations based on the particles-in-cell (PIC) method [129, 130]. Computer simulation possessing almost unlimited diagnostic capabilities of the processes in relativistic plasmas shows how to choose the parameters of the laser pulse and the target in order to provide the conditions under which the protons are accelerated to the energy of several hundred MeV with the number of accelerated particles per laser pulse ranging $10^{11} - 10^{13}$.

Here, we mention the basic mechanisms of ion acceleration accompanying the interaction of laser radiation with solid and gas targets. The fundamental difference between solid targets and gas targets is that the electron density in the solid targets is so high that such targets are not transparent to laser radiation. In other words, the electron density exceeds the critical density $n_{\mathrm{crit}} = m_{\mathrm{e}}\omega^2/4\pi e^2$ for radiation with the frequency ω. In the gas target, the ionization of a gas by laser radiation leads to the formation of plasma with a subcritical density — that is, the target is transparent to the laser pulses. Plasma with a near-critical density can be produced by irradiating a solid target with a prepulse that precedes the main laser pulse; an amplitude of the former is many orders of magnitude smaller, but its duration is many orders of magnitude greater than the latter. Thus, the prepulse energy transferred to the target is not negligibly small and should be taken into account. Due to its relatively long duration, the formation of a plasma corona occurs with a size substantially larger than the initial target thickness, which, in turn, has a significant impact on the whole process of interaction [131, 132]. In particular, the plasma corona may absorb a substantial part of the laser pulse energy, with the result that plasma electrons are heated [133, 134], and their energy can then be transferred to the ions.

In the process of solid target irradiation by a powerful laser, the ion acceleration occurs in the following modes: via the Coulomb explosion; in the electric field of charge separation on the target surface, and by the radiation pressure of a strong electromagnetic wave.

4.1 Coulomb explosion

Apparently, from the point of view of a theoretical description, the Coulomb explosion is the simplest collective mechanism of ion acceleration [135–137]. In this mode, almost all of the electrons are removed from the focus area of the irradiated target under the action of ponderomotive pressure of the laser radiation. The remaining ion core expands (explodes) due to the Coulomb repulsion of positive electric charges. In the purest form, the Coulomb explosion mode can be realized in the interaction of laser radiation with clusters [136–139]. The clusters constitute clumps of matter of solid-state density and micron size [140]. Usually, they are formed during gas expansion into a vacuum. The typical distance between the individual clusters measures several micrometers.

As a result of cluster irradiation, the electrostatic potential is created when electrons are ejected under the action of the ponderomotive force of the laser radiation. Its maximum value equals the electrostatic potential on the surface of the charged sphere with radius $R_{\rm cl}$ and the density of charged particles $n_{0,\alpha}$:

$$\varphi_{\max} = 2\pi n_{0,\alpha}\,\frac{eR_{\rm cl}^2}{3}\,. \tag{16}$$

Assuming that the ion temperature is equal to zero and that the ions move along the radius, we can find the ratio between the ion kinetic energy

$$\mathcal{E} = \sqrt{m_\alpha^2 c^4 + p_r^2 c^2} - m_\alpha c^2 \tag{17}$$

and the ion potential energy

$$\Pi(r_0, t) = 4\pi e^2 Q(r_0)\left(\frac{1}{r_0 + \xi_\alpha(r_0,t)} - \frac{1}{r_0}\right), \tag{18}$$

which corresponds to the energy integral $\mathcal{E} + \Pi(r_0,t) = \text{const}$. Here, r_0 is the initial ion coordinate, $\xi_\alpha(r_0,t)$ is the ion displacement at the instant of time t from the initial position, and the number of particles $Q(r_0)$ within the sphere of radius r_0 equals

$$Q(r_0) = \int_0^{r_0} n_{0,\alpha}(r)\,r^2\,\mathrm{d}r\,. \tag{19}$$

In the process of ion cloud expansion, the kinetic energy increases, reaching the value of $4\pi e^2 Q(r_0)/r_0$ in the limit $\xi_\alpha \to \infty$. The energy of an ion is determined by the coordinate of its initial position inside the cloud. Assuming that the ion density $n_{0,\alpha}$ inside the cloud is homogeneous, we arrive at the final ion energy $\mathcal{E}_\alpha = 2\pi e^2 n_{0,\alpha} r_0^2/3$, which cannot exceed $\mathcal{E}_{\alpha,\max} = 2\pi e^2 n_{0,\alpha} R_{\rm cl}^2/3$. Using the fact that the ion energy is proportional to r_0^2, we can find the ion energy spectrum $\mathcal{N}_\alpha(\mathcal{E}) = \mathrm{d}f_\alpha/\mathrm{d}\mathcal{E}$, which by virtue of the flux conservation in the phase space is equal to $4\pi r_0^2\,\mathrm{d}r_0/\mathrm{d}\mathcal{E}$. From this, it follows that [136]

$$\mathcal{N}_\alpha(\mathcal{E}) = \frac{3R}{2Z_\alpha^2 e^2}\sqrt{\frac{\mathcal{E}}{\mathcal{E}_{\alpha,\max}}}\,\theta(\mathcal{E}_{\alpha,\max} - \mathcal{E})\,, \tag{20}$$

where $\theta(x)$ is the above-defined unit step Heaviside function. An energy spectrum of this form has been obtained in three-dimensional particle-in-cell simulations of the cluster Coulomb explosion [136, 141]. It has also been demonstrated in experiments [142] with the cluster targets irradiated by high-intensity laser radiation.

In the limit of relatively low ion energy, $\mathcal{E}_\alpha < m_\alpha c^2$, we can rely on a nonrelativistic description of the Coulomb explosion. Within the framework of this approximation, the solution of the equations of motion can be written out in the Lagrange variables r_0, t as

$$\frac{1}{2}\ln\frac{2\xi_\alpha + r_0 + 2\sqrt{\xi_\alpha^2 + r_0\xi_\alpha}}{r_0} + \frac{\sqrt{\xi_\alpha^2 + r_0\xi_\alpha}}{r_0} = \sqrt{\frac{2}{3}}\,\omega_{\rm p\alpha}t\,. \tag{21}$$

On the right hand side of Eqn (21), $\omega_{\rm p\alpha} = \sqrt{4\pi n_{0,\alpha}Z_\alpha e^2/m_\alpha}$ is equal to the ion plasma frequency. When the displacement is small, $\xi_\alpha \ll r_0$, the ions move with constant acceleration, $\xi_\alpha \approx r_0(\omega_{\rm p\alpha}t)^2/6$, while in the limit $\xi_\alpha \to \infty$ we have $\xi_\alpha \approx \sqrt{2/3}\,r_0\omega_{\rm p\alpha}t$. In the latter case, the ion velocity is constant. The characteristic time of ion cloud expansion is equal to an order of magnitude to the inverse value of the ion plasma frequency, $\omega_{\rm p\alpha}^{-1}$. We have been assuming above that the Coulomb explosion of the cluster is spherically symmetric. The effects of cluster asymmetry have been discussed in Refs [143–145]. The asymmetry of the Coulomb explosion is related to the edge intensification of the electric field. As is known, the field amplitude in a uniform electric field at the poles of a conducted sphere is twice its value at the equator. In the case of an elongated ellipsoid, the difference between the values of the field is significantly larger, being proportional to the ratio of the major-to-minor semiaxes of the ellipsoid. This effect leads to ion injection into the accelerating electric field from the near-polar regions.

Let us consider ion acceleration in a multispecies cluster, assuming that the concentration of the ion species is relatively small: $Z_\beta n_\beta \ll Z_\alpha n_\alpha$. Here, $Z_\beta e$ and n_β are the electric charge and number density of the minor species ions. Within the framework of this approximation, the dynamics of impurity ions can be described as the motion of a test particle in a given electric field generated by the spatial distribution of the electric charges of the main component ions. Solving the problem of ion motion in this electric field, one can show that the energy spectrum of the impurity ions has the form [146]

$$\mathcal{N}_\beta(\mathcal{E}) = \frac{3R\sqrt{\mathcal{E}_{\beta,\max} - \mathcal{E}}}{\sqrt{2\mathcal{E}_{\beta,\max}}\,Z_\alpha Z_\beta e^2}\,\frac{n_{0,\beta}}{n_{0,\alpha}}\,\theta(\mathcal{E}_{\beta,\max} - \mathcal{E})\,\theta(\mathcal{E} - \mathcal{E}_{\beta,\min})\,, \tag{22}$$

where the maximum and minimum energies are equal to

$$\begin{aligned}\mathcal{E}_{\beta,\max} &= \frac{8\pi Z_\alpha Z_\beta e^2 n_{0,\alpha} R^2}{3}\,,\\ \mathcal{E}_{\beta,\min} &= \frac{4\pi Z_\beta e^2 R^2}{3}\,(Z_\alpha n_{0,\alpha} - Z_\beta n_{0,\beta})\,.\end{aligned} \tag{23}$$

As an illustration of ion acceleration in the process of a Coulomb explosion of the cluster, we present in Fig. 8 the results of computer simulations of laser radiation interacting with the cluster applying the particles-in-cell method. Here and below, the electromagnetic, relativistic PIC code REMP is used [147]. The laser pulse linearly polarized with the electric field parallel to the z-axis propagates in the x direction. Its normalized amplitude is equal to 10, which corresponds to the radiation intensity $I = 1.37\times10^{20}$ W cm^{-2}. A cluster comprising electrons and protons ($m_\alpha/m_{\rm e} = 1836$) has 0.2 μm in diameter. The initial distribution of the plasma density, equal to $100n_{\rm crit}$ at $t = 0$, is uniform inside the cluster. The simulation has been carried out on mesh $1024\times1024\times1024$ in size. The total particle number reaches 3×10^6. The top row shows the spatial distribution of electrons and protons in consecutive

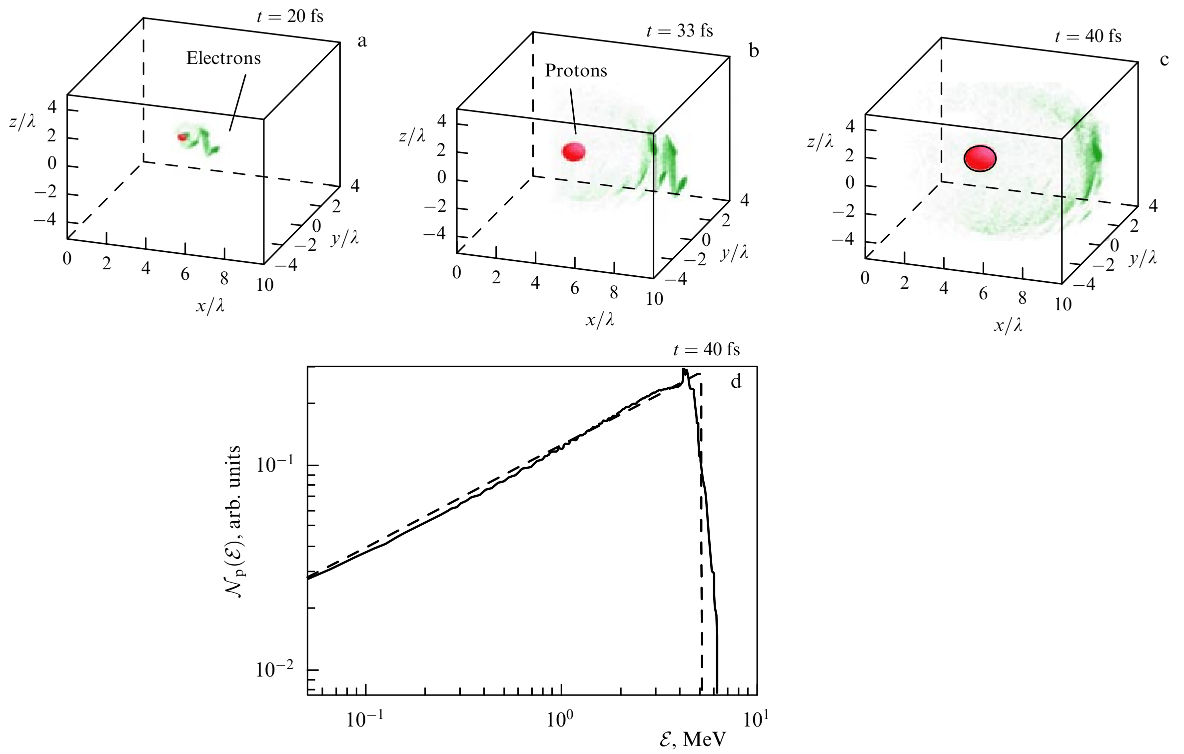

Figure 8. Interaction of laser radiation with a cluster. Top row: (a)–(c) Distributions of electrons and protons at consecutive instants of time. Bottom row: (d) Energy spectrum of protons at time $t = 40$ fs. The dashed line shows the spectrum described by formula (20).

moments of time. It is seen that the electrons are 'blown off' by the electromagnetic wave in the direction of the wave propagation. The cloud of remaining protons expands with a small deviation from the spherical symmetry. In the lower part of the figure, we show the energy spectrum of protons at time $t = 40$ fs. The dashed line depicts the spectrum described by formula (20).

When the density distribution within a cluster is not uniform, the Coulomb explosion leads at some instant of time to the formation of a singularity in the ionic component. The singularity corresponds to a specific type of gradient catastrophe. As a result of the singularity development, the velocity gradient and the density of ions become infinite at some coordinate [138, 148, 149].

Figure 9 displays the density distribution of ions and the profile of their velocities for time instants before and during the formation of the singularity in the ion density.

In the initial configuration at $t = 0$, the ion density dependence on the radius in the spherically symmetric cluster is given by the expression $n_\alpha(r_0) = (4/\pi^{1/2}R^3) \times \exp(-r_0^2/R^2)$. The initial radius of the cluster is $R = 0.5$ μm. As is seen in Fig. 9, the ion cloud expands with a velocity proportional to the radius in the region close the cluster center. At some distance from the cluster center, the ion velocity reaches a maximum and then decreases. As a consequence, the internal ion layers move faster than the ions at the periphery of the cluster, leading to a steepening of the ion velocity profile and to the formation of singularity in the density distribution of the ions at some instant of time. This singularity is integrable: although the density tends to infinity at some surface, it contains a finite number of particles in its vicinity.

The singularity formation, which corresponds to the maximum of the ion velocity, results in the quasimonoenergetic ion energy spectrum. The energy spectrum of the ions has the form $\mathcal{N}_\alpha(\mathcal{E}) \propto 1/\sqrt{\mathcal{E}_{\alpha,\max} - \mathcal{E}}$.

Ion acceleration through the Coulomb explosion mechanism is realized under the condition that the electric field of the laser radiation exceed the value of the electric field on the surface of the cluster: $E_{\rm las} > 4\pi n_{0,\alpha} e R_{\rm cl}/3$. It can be rewritten as $a > \omega_{\rm pe}^2 R_{\rm cl}\lambda/6\pi c^2$. The maximum energy of accelerated ions is given by the expression $\mathcal{E}_\alpha = m_e c^2 \omega_{\rm pe}^2 R_{\rm cl}^2/6c^2$. In the context of an application to hadron therapy, where a proton energy of about 200 MeV is required, for a solid-state density cluster, $n_{0,\alpha} \approx 10^{23}$ cm^{-3}, we obtain the estimates of necessary parameters: the cluster size is $R_{\rm cl} \approx \lambda \approx 1$ μm, and the number of accelerated particles per cluster is $N \approx 4 \times 10^{12}$. For the required normalized laser field amplitude, this yields $a > 200$, i.e., the radiation intensity should be on the order

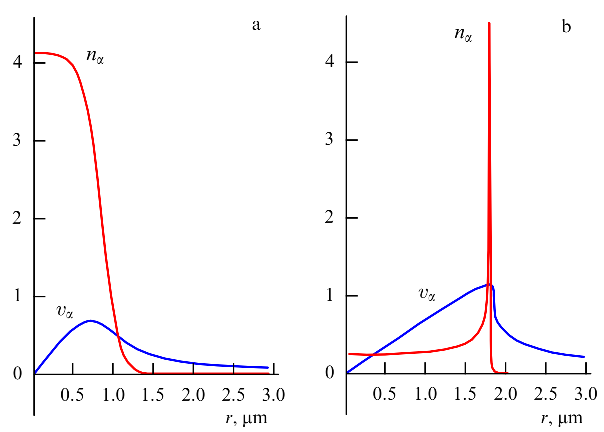

Figure 9. Radial density distribution of ions and the profile of ion velocity (in arb. units) inside a cluster for time (a) $t = 0.5$, and (b) $t = 1.5$.

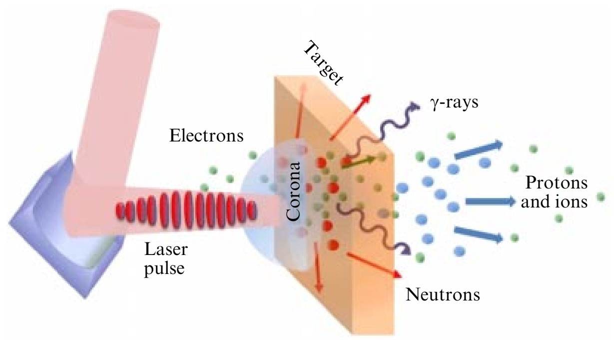

Figure 10. Ion acceleration in the target near-surface layer. A relatively long, small-amplitude prepulse creates a plasma corona on the target's front side. The main laser pulse generates in the plasma corona high-energy electrons which penetrate through the dense target. The acceleration of ions in the near-surface layer on the target's rear side occurs in the electric field which is generated by fast electrons. The interaction of laser radiation with solid targets is also accompanied by the generation of gamma-rays, neutrons, positrons, and other debris from nuclear reactions.

of 5×10^{22} W cm^{-2}, which corresponds to a petawatt class laser.

The cluster targets provide a convenient example for explaining the basic features of a simple collective ion acceleration mechanism by laser radiation. However, further study is needed to clarify the conditions under which the cluster targets can be employed in medical laser accelerators. Because of the transverse inhomogeneity of the radiation intensity in the laser beam due to the required tight focusing, the irradiation conditions of different clusters are very distinct. This should inevitably lead to the generation of broad ion energy spectra. In addition, the accelerated ions in the Coulomb explosion of a spherical cluster have an isotropic distribution, while in hadron therapy the collimated ion beams are required. Using certain devices, which are discussed below in Section 5.1, a collimated ion beam can be prepared, but this will lead to enhanced complexity of the facility and will reduce the efficiency of laser energy conversion into the energy of fast ions.

4.2 Ion acceleration in a target near-surface layer

The next acceleration mechanism corresponds to the case when ions are accelerated by a charge-separated electric field at the front of a plasma cloud expanding into a vacuum. A strong electric field is induced inside the layer produced by hot electrons at the target rear side with respect to the direction of the laser pulse propagation [96, 150]. This is the so-called target normal sheath acceleration (TNSA) mechanism, which is typically realized in experiments on studying the process of moderate intensity laser radiation interaction with thin metallic or/and plastic foil targets. In the experiments, fast protons are usually detected, whose appearance in the case of metal foils is explained by the presence of a nanometer-thick water contamination layer on the target surface.

A schematic description of this acceleration mechanism is presented in Fig. 10. The mechanism can be realized both in static and in dynamic modes.

4.2.1 Static mode of ion acceleration. In the process of laser radiation interaction with a thin target, the electrons are heated on the front target surface relative to the direction of the laser pulse propagation. Fast electrons propagate through the target, and leaving it form a layer with a high positive electric field at the rear side of the target; this field accelerates the ions, as shown in Fig. 10. In order to find the electric field distribution in the near-surface layer, it is necessary to solve the Poisson equation

$$\frac{\mathrm{d}^2\phi}{\mathrm{d}x^2} = n_{\mathrm{e,h}}(\phi) - \theta(-x)\,, \tag{24}$$

where $n_{\mathrm{e,h}}$ is the number density of hot electrons. This equation is written in dimensionless variables. The electrostatic potential ϕ is normalized to $T_{\mathrm{e,h}}/e$, where $T_{\mathrm{e,h}}$ is the temperature of fast electrons. The hot electron density and the density of the positive electric charge, being proportional to the difference between the ion concentration and the concentration of cold electrons, are normalized to $\delta n_{0,\alpha}$. The spatial coordinate is measured in units of the Debye radius $r_{\mathrm{D,e}} = \sqrt{T_{\mathrm{e,h}}/4\pi\delta n_{0,\mathrm{e}}e^2}$ with characteristic electron density $\delta n_{0,\mathrm{e}}$, which in the limit $x \to -\infty$ is equal to the density of the positive electric charge. The unit step Heaviside function, $\theta(x)$, describes the profile of the target positive electric charge. The ions are assumed to be at rest. For the sake of simplicity, we neglect the influence of the cold background electrons on the electrostatic potential distribution, referring, for example, to paper [151], where appropriate analysis has been conducted. The dependence of electron density on the electrostatic potential on the right-hand side of Eqn (24) is determined by the electron distribution function.

The widely accepted approximation employed in publications devoted to ion acceleration by the charge-separated electric field assumes that the energy distribution of electrons obeys the Boltzmann law. Within the framework of the one-dimensional geometry approximation, the Boltzmann distribution function of the electrons leads to an infinite energy of accelerated ions [152]. The reason for this is the presence of electrons with formally infinite energy in the electron distribution, which results in electrostatic potential dependence on the coordinate described by the function which tends to infinity logarithmically in the limit $x \to \infty$. In the case of conditions more realistic for the interaction of short laser pulses with various targets, the electron distribution is terminated at some maximum energy which is equal to an order of magnitude to the energy of electron quivering in the laser radiation field. As shown in Refs [153, 154], such distribution functions lead to the dependence of fast electron density on the potential, $n_{\mathrm{e}}(\phi)$, in a form corresponding to the so-called Kappa-function:

$$n_{\mathrm{e,h}}(\phi) = \left(1 + \frac{\kappa - 1}{\kappa}\,\phi\right)^{1/(\kappa-1)}, \tag{25}$$

where the power index is determined by the specific form of the electron distribution function [155, 156].

Formally, relationship (25) corresponds to a politropic dependence of the electron gas pressure on the density: $p = p_0(n/n_0)^{\kappa}$. In the particular case of $\kappa = 3$, the electron energy distribution is described by the function which takes a constant value for energies smaller than the maximum value of $\mathcal{E}_{\mathrm{e,max}} = \kappa/(\kappa - 1)\,T_{\mathrm{e,h}}$, and vanishes for $\mathcal{E}_{\mathrm{e}} > \mathcal{E}_{\mathrm{e,max}}$.

Referring to Fig. 11, we present the results of a numerical solution of Eqn (24) for the boundary conditions of $\phi \to 0$ as $x \to -\infty$, and $\mathrm{d}\phi/\mathrm{d}x \to 0$ in the limit $x \to \infty$. Figure 11a shows the dependence of the positive electric charge in the target, $\delta n_{0,\alpha}(x)$ (dashed curve), of the hot electron density $n_{\mathrm{e,h}}(x)$, of the electric field strength $E(x)$, and of the

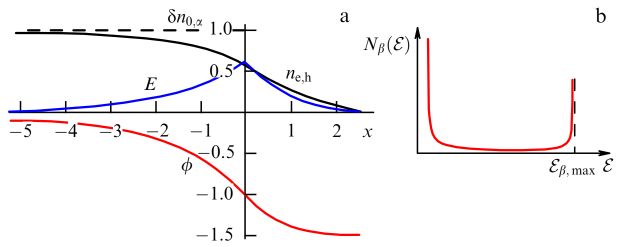

Figure 11. (a) Dependence of the positive charge distribution inside the target, $\delta n_{0,\alpha}$ (dashed line), the hot electron density $n_{e,h}$, the electric field E, and electrostatic potential ϕ on the coordinate x for the power index equal to $\kappa = 3$. (b) Energy spectrum of fast ions.

electrostatic potential $\phi(x)$ for the politropa index $\kappa = 3$. In the region of $x \geqslant 0$, the electron density and the electric field vanish at a finite distance from the target surface. Here, the electrostatic potential takes the following value: $\phi_{\max} = -\mathcal{E}_{\alpha,\max}/Z_\alpha e = -[\kappa/(\kappa-1)]T_{e,h}/Z_\alpha e$.

Describing the ion acceleration of a β species within the framework of the test particle approximation, i.e., by considering the ion motion in a given electric field, allows finding the energy spectrum of ions $\mathcal{N}_\beta(\mathcal{E})$. It has the form

$$\mathcal{N}_\beta(\mathcal{E}) \propto \frac{1}{(\mathcal{E}_{\beta,\max} - \mathcal{E})^s}\,, \tag{26}$$

with the power index $s = \kappa/[2(\kappa-1)]$ (see Fig. 11 b). If $\kappa = 3$, the index s is equal to $3/4$. The ion energy spectrum has an integrable singularity at $\mathcal{E} = \mathcal{E}_{\beta,\max}$.

We note here that for the Maxwell distribution of hot electrons, which leads to the dependence $n_e(\phi) = \exp(-\phi)$ on the right-hand side of equation (24), being a limit of the function (25) as $\kappa \to 1$, the ion energy spectrum takes an exponential form.

4.2.2 Dynamic mode of ion acceleration. In the dynamic mode, the ions are accelerated by an electric field induced due to the electric charge separation in the layer at the front expanding into a vacuum plasma cloud [157–163]. Within the framework of the approximation, assuming plasma charge quasineutrality, when $n_\alpha = n_{e,h} = n$, the ion motion is described by the system of equations

$$\partial_t n + \partial_x (nv) = 0\,, \tag{27}$$

$$\partial_t v + v\,\partial_x v = \partial_n \phi\,\partial_x n\,. \tag{28}$$

On the right-hand side of Eqn (28), the derivative of the potential with respect to the density is $\partial_n \phi = \mathrm{d}n/\mathrm{d}\phi$, with the function $n(\phi)$ given by Eqn (25). The ion velocity v is normalized to the ion sound speed $c_s = \sqrt{T_{e,h}/m_\alpha}$. (Regarding the ion acceleration in multispecies plasmas, see, for example, Ref. [164].)

The general approach to solving such systems of hydrodynamic type equations is described in book [165]. The self-similar solution of Eqns (27) and (28), in which the functions n and v depend on the variable $\zeta = x/c_s t$, obeys the system of ordinary differential equations

$$(v - \zeta)\,n' = nv'\,, \tag{29}$$

$$(v - \zeta)\,v' = \partial_n \phi\, n'\,, \tag{30}$$

where the prime denotes differentiation with respect to ζ. The existence condition of nontrivial solutions to the system of linear algebraic equations (29) and (30) is that the appropriate determinant vanishes:

$$(v - \zeta)\,v' - \partial_n \phi\, n' = 0\,. \tag{31}$$

This condition yields the relationships

$$v - \zeta = \sqrt{n\,\partial_n \phi}\,, \quad \frac{\mathrm{d}n}{\mathrm{d}v} = \sqrt{\frac{n}{\partial_n \phi}}\,. \tag{32}$$

Using them for $\kappa = 3$, it is possible to represent the solution of equations (29) and (30) as

$$v = \frac{c_s}{2}\left(\frac{x}{c_s t} + \sqrt{3}\right), \tag{33}$$

$$n = \frac{n_0}{2}\left(1 - \frac{1}{\sqrt{3}}\frac{x}{c_s t}\right). \tag{34}$$

For a known electron density, the electrostatic potential is given by the expression $\phi = (3/2)(n^2 - 1)$.

For a self-similar variable, which takes the value of $\zeta = \sqrt{3}$, the ion density vanishes. Here, the fast ion energy passes through a maximum $\mathcal{E}_{\beta,\max} = (3/2)T_{e,h}$ (see also Ref. [166]). In the vicinity of the maximum energy, the energy spectrum of fast ions has the form

$$\mathcal{N}_\beta(\mathcal{E}) \propto \frac{2\sqrt{2}}{\sqrt{\mathcal{E}_{\beta,\max} - \mathcal{E}}}\,. \tag{35}$$

In this expression, the singularity appearing as $\mathcal{E} \to \mathcal{E}_{\beta,\max}$ is also integrable.

In the above expressions, the typical ion energy is determined by the effective temperature of the electrons, or more precisely, by their average kinetic energy. Electron heating can occur in the plasma corona and/or on the solid target surface. Different mechanisms have been considered in order to describe the electron heating. In the plasma corona, the heating of electrons can occur due to the nonresonance absorption [167], as well as due to the resonance mechanism inside the self-focusing channel [168] or in the plasma critical density layer in the plasma resonance region [169, 170]. The electrons can acquire energy at the plasma–vacuum interface due to so-called 'vacuum heating' [171, 172]. As a result, the electron temperature becomes equal, to an order of magnitude, to the kinetic energy of the electron quivering in the laser radiation field, which gives

$$T_{e,h} = m_e c^2\left(\sqrt{1 + a_0^2} - 1\right), \tag{36}$$

where the normalized amplitude of the laser field is given by

$$a_0 = \frac{eE}{m_e \omega c} = \sqrt{\frac{I\lambda^2}{1.37 \times 10^{18}\ \mathrm{W\,cm^{-2}}}}\,. \tag{37}$$

Here, I is the laser intensity. From this follows the proportionality of the maximum energy of fast ions to the square root of the laser radiation intensity: $\mathcal{E}_{\max} \propto \sqrt{I\lambda^2}$, observed in experiments whose results are collected in Fig. 7a.

When the electrons possess the Maxwell distribution over the energy, the ion energy spectrum also has an exponential form with a characteristic energy proportional to the electron temperature, i.e., proportional to the square root of the laser radiation intensity.

We note that according to the relationships found above for achieving an energy of accelerated protons equal to 200 MeV, it may be required that the laser intensity on the target be on the order of 10^{23} W cm^{-2}, which corresponds to petawatt class lasers.

4.3 Ion acceleration by light radiation pressure

Among other mechanisms of acceleration in the laser high-intensity limit, the mechanism of ion acceleration by radiation pressure [98, 173, 174], when an irradiated thin target moves as a whole under the radiation pressure exerted by an electromagnetic wave, has the greatest efficiency. This acceleration mechanism has attracted increasing attention both in theoretical and in experimental work owing to the fact that it predicts the generation of high-quality ion beams with a high efficiency of laser energy conversion into the energy of accelerated ions.

The force acting on the target is equal to the momentum flux of an electromagnetic wave, which is proportional to the Poynting vector: $\mathbf{S} = c\mathbf{E}\times\mathbf{B}/4\pi$. For the sake of simplicity, we also assume that the electromagnetic wave is circularly polarized, has the frequency ω and wave vector $\mathbf{k}$, and propagates along the x-axis. The wave is given by the vector potential

$$\mathbf{A} = A_0\left[\cos(\omega t - kx)\mathbf{e}_y + \sin(\omega t - kx)\mathbf{e}_z\right], \tag{38}$$

where $\mathbf{e}_y$ and $\mathbf{e}_z$ are unit vectors along the y- and z-axes, and $k = |\mathbf{k}|$ is the wave number. Calculating the electric, $\mathbf{E} = -\partial_t\mathbf{A}/c$, and magnetic, $\mathbf{B} = \nabla\times\mathbf{A}$, fields, we find the Poynting vector

$$\mathbf{S} = c\omega k A_0^2\mathbf{e}_x \tag{39}$$

proportional to the product of the frequency ω and the wave number k. In the frame of reference moving with the target velocity $v = \beta c$, the product of the frequency and the wave number is given by the expression

$$\begin{aligned}\bar{\omega}\bar{k} &= \omega k\,\frac{1+\beta^2}{1-\beta^2} - (\omega^2 + k^2)\,\frac{\beta}{1-\beta^2}\\ &= \omega^2\,\frac{(\beta_{\mathrm{g}}-\beta)(1-\beta_{\mathrm{g}}\beta)}{1-\beta^2}\,.\end{aligned} \tag{40}$$

In order to derive this expression, we have used the relationship between the frequency, wave number, and group velocity of an electromagnetic wave: $v_{\mathrm{g}} = c\beta_{\mathrm{g}} = kc^2/\omega$, where $\beta_{\mathrm{g}} = v_{\mathrm{g}}/c$ is the normalized group velocity.

Summing up the values of the Poynting vector in the incident and reflected waves and subtracting the value of the Poynting vector in the transmitted wave, we find the force acting on the target. It is given by the expression

$$F = \left(1 + |\rho|^2 - |\tau|^2\right)S\,, \tag{41}$$

where $|\rho|^2$ and $|\tau|^2$ are the reflection and transmission coefficients of the electromagnetic wave. They are connected by the relationship

$$|\rho|^2 + |\tau|^2 + |\alpha|^2 = 1\,. \tag{42}$$

Here, $|\alpha|^2$ is the absorption coefficient. Using expressions (39)–(42), we find that the equation of motion of the surface element of a thin target can be written in the form [123]

$$\frac{1}{(1-\beta_\alpha^2)^{3/2}}\,\frac{\mathrm{d}\beta_\alpha}{\mathrm{d}t} = \frac{KE^2}{4\pi\sigma_0 m_\alpha c}\,\frac{(\beta_{\mathrm{g}}-\beta_\alpha)(1-\beta_{\mathrm{g}}\beta_\alpha)}{1-\beta_\alpha^2}\,, \tag{43}$$

where $K = 2|\rho|^2 + |\alpha|^2$, and $\sigma_0 = n_0 l_0$ is equal to the surface density of the target with the thickness l_0. In Eqn (43), $\beta_\alpha = p_{\alpha,x}/(m_\alpha^2c^2 + p_{\alpha,x}^2)^{1/2}$ is the x-component of the normalized velocity of the surface element of the target, and $E^2 = (\omega A/c)^2$. As is seen, the radiation pressure vanishes in the limit $\beta_\alpha \to \beta_{\mathrm{g}}$. This constraint must be taken into account for sharply focused laser pulses. In the case of complete absorption of radiation by the target, which corresponds to the equalities $|\rho|^2 = 0$ and $|\alpha|^2 = 1$, the radiation pressure on the target is half that of a perfectly reflective target, when $|\rho|^2 = 1$ and $|\alpha|^2 = 0$, which is in agreement with general relationships formulated in book [124]. A detailed analysis of target opacity effects on ion acceleration can be found in articles [175–178].

In the case of a laser pulse with a constant amplitude ($E = \mathrm{const}$), the solution of equation (43) can be written in the form [177]

$$\begin{aligned}&\ln\frac{1-\beta\beta_{\mathrm{g}} + \beta(1-\beta_{\mathrm{g}}^2)^{1/2}(1-\beta^2)^{1/2}}{(\beta_{\mathrm{g}}-\beta)\left[1+(1-\beta_{\mathrm{g}}^2)^{1/2}\right]}\\ &\quad - \beta_{\mathrm{g}}\left[\arctan\frac{(1-\beta_{\mathrm{g}}^2)^{1/2}(1-\beta^2)^{1/2}}{\beta_{\mathrm{g}}-\beta} - \arccos\beta_{\mathrm{g}}\right]\\ &\quad = \beta_{\mathrm{g}}(1-\beta_{\mathrm{g}}^2)^{3/2}\,\frac{KE^2}{4\pi\sigma_0 m_\alpha c}\,t\,.\end{aligned} \tag{44}$$

The main parameter characterizing the radiation mechanism of ion acceleration is proportional to the fluence of the electromagnetic wave (it is the integral of the momentum flux through a target unit surface):

$$w = \int_{-\infty}^{\psi}\frac{KE_{\mathrm{las}}^2}{4m_\alpha\sigma_0\omega^2\lambda}\,\mathrm{d}\psi\,. \tag{45}$$

In this expression, the fluence $w(\psi)$ is written out in the dimensionless form. It is a function of the wave phase $\psi = \omega(t - x/c)$, where the coordinate $x(t)$ of the target must be found by solving the equations of motion. Furthermore, we assume that $\beta_{\mathrm{g}} = 1$, and for fluence w we take its value in the limit $\psi\to\infty$: $w = w(\psi)|_{\psi=\infty}$.

As follows from publications [98–101], the dependence of the accelerated proton energy (here, we take $\alpha = \mathrm{p}$) on the fluence w is given by the expression

$$\mathcal{E}_{\mathrm{p}} = m_{\mathrm{p}}c^2\,\frac{2w^2}{1+2w}\,. \tag{46}$$

In other words, the energy of accelerated ions for a fixed pulse length is proportional in the nonrelativistic limit ($w \ll 1$) to the square of the radiation intensity.

The conversion efficiency of laser energy into the energy of fast particles is $\kappa_{\mathrm{eff}} = \mathcal{E}_{\mathrm{las}}/\mathcal{N}_{\mathrm{p}}\mathcal{E}_{\mathrm{p}}$, where $\mathcal{N}_{\mathrm{p}}$ is the total number of accelerated particles, and $\mathcal{E}_{\mathrm{las}} = \int(E^2/4\pi)\,\mathrm{d}V$ is the laser pulse energy, which takes the form

$$\kappa_{\mathrm{eff}} = \frac{2w}{1+2w}\,. \tag{47}$$

Using relationships (46) and (47), we can show that generating $\mathcal{N}_{\rm p} = 5 \times 10^{11}$ protons per second (one of the requirements specified by hadron therapy for the parameters of the laser accelerator) with the particle energy equal to 250 MeV requires lasers with the repetition rate of 1 Hz and with an energy per pulse of $\mathcal{E}_{\rm las} = 40$ J. If the pulse duration equals 30 fs, then for the laser power we obtain a value of order 1 PW. The acceleration efficiency $\kappa_{\rm eff}$ in this case amounts to 0.5.

To implement the optimal acceleration mode, we should choose the thickness of the target to be on the opacity threshold for laser radiation [178, 179], which assumes that the laser pulse amplitude has to satisfy the condition

$$a_0 \leqslant \epsilon_{\rm p} \, . \tag{48}$$

Here, the amplitude a_0 is related to the vector potential A_0 by the formula $a_0 = eA_0/m_{\rm e}c^2$. The dimensionless parameter $\epsilon_{\rm p} = 2\pi ne^2 l_0/m_{\rm e}\omega c$ was introduced in paper [180]. It characterizes the relativistic transparency threshold of a thin plasma layer. For example, if a petawatt laser pulse is focused on the region of size 3 μm, i.e., the laser intensity reaches the level of $I = 10^{21}$ W cm^{-2}, the thickness of a solid density foil target with an electron number density of about $n_{\rm e} \sim 10^{23}$ cm^{-3} should be equal to 0.2 μm.

An additional constraint on the target and laser parameters stems from the requirement of a very high quality of the accelerated ion beam (the issues related to the ion beam quality are discussed in more detail below). The beam must have a small spread in energy. The transverse inhomogeneity of the laser radiation intensity and, therefore, of the fluence inhomogeneity determines the dependence of the accelerated ion energy on the transverse coordinate.

Taking into account the beam laminarity, it is possible to select a group of ions in the paraxial region with a small energy spread. In accordance with the theoretical and simulation predictions, the ion beam has the form of a thin shell whose element velocity is maximum on the axis. In the paraxial region, the dependence of the ion energy on the radius r can be approximated by the function

$$\mathcal{E}_\alpha(r) = \mathcal{E}_{\alpha,\,\max}\left(1 - \frac{r^m}{R_\perp^m}\right), \tag{49}$$

with the index m equal to 2 for a laser pulse with a Gaussian profile, and with $m > 2$ for pulses described by a super-Gaussian function. It is assumed that the laser pulse has a radius $R_\perp$.

To generate a high-quality beam, we can use a screen with a small aperture. The radius of the hole Δr is related to the ion beam energy width $\Delta\mathcal{E}_\alpha$ by the expression

$$\Delta r = R_\perp\left(\frac{\Delta\mathcal{E}_\alpha}{\mathcal{E}_{\alpha,\,\max}}\right)^{1/m}. \tag{50}$$

Hence it follows that, in order to obtain a beam with a narrow energy spectrum bounded by $\Delta\mathcal{E}_\alpha/\mathcal{E}_{\alpha,\,\max} \leqslant 2\%$, we need to have $\Delta r/R_\perp \approx 0.14$ if the index equals $m = 2$, and $\Delta r/R_\perp \approx 0.38$ for $m = 4$. Using Eqns (48)–(50), we find that the required energy and power of the laser radiation must be equal to 75 J and 2.5 PW in the case of a Gaussian pulse, and to 20 J and 700 TW if $m = 4$.

4.4 Parameters corresponding to different mechanisms of ion acceleration from thin foil targets

As was shown in Section 4.1, the ion acceleration mode in the process of Coulomb explosion can be realized if the laser pulse has a sufficiently large intensity, provided the surface density of the target, $\sigma_0 = n_0 l_0$, is not too large. In the opposite limit of high target surface density and a relatively small electromagnetic wave intensity, a slow heating of the electrons occurs. In this case, the mechanism of ion acceleration at the front of the plasma cloud becomes valid.

The boundary between these two regimes in the parameter plane 'radiation amplitude–target surface density' is given by condition (48), which can be represented in the form $a_0 = \sigma_0 \lambda r_{\rm e}$. Here, $r_{\rm e} = e^2/m_{\rm e}c^2 = 2.8 \times 10^{-13}$ cm is the classical electron radius. Condition (48), as was noted above, also determines the region of parameters where the radiative acceleration of ions comes into play. The regions in the parameter plane 'amplitude–surface density', corresponding to the acceleration of ions in the interaction of laser radiation with thin foils, are shown schematically in Fig. 12.

4.5 Intermediate regimes

Combining the above basic acceleration modes, it is possible to obtain ion beams with even higher energies. This is exemplified by a mechanism called 'directed Coulomb explosion' [181–183]. In PIC simulations [181, 182], a linearly polarized sharply focused ($f/D = 1.5$) laser pulse (15 J, 30 fs, 500 TW, wavelength $\lambda = 1$ μm) interacts with a thin double-layer target. The electron number density in the first Al^{+13} layer with a thickness of 0.1λ and lateral size of 9λ is equal to $400\,n_{\rm cr}$. In the second H^+ layer, with a thickness of 0.05λ and lateral size of λ, the electron density equals $30\,n_{\rm cr}$. During interaction with the laser light at the initial stage, section of the thin foil is accelerated by the laser radiation pressure. Then, the electrons are displaced from the domain of interaction of laser radiation with the target, and the remaining ion core 'explodes'. Since at the beginning of this process the ions have a finite longitudinal momentum, the Coulomb explosion occurs in an anisotropic way. As a result, the ions originated from the target rear side and accelerated by a moving potential acquire higher energy. Since few electrons remain in the interaction region at this stage, the expanding target becomes transparent to the laser radiation.

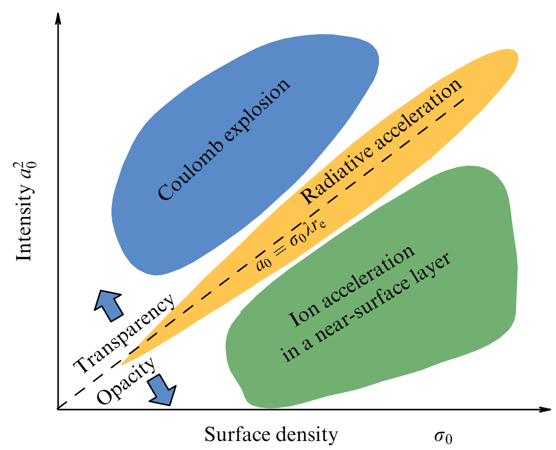

Figure 12. Regions in the parameter plane 'amplitude–surface density', corresponding to the acceleration of ions during laser radiation interaction with thin foils in the regimes of Coulomb explosion, TNSA, and radiation pressure acceleration.

The laser pulse passes through the plasma layer and provides additional energy to the preaccelerated ions in direct mode acceleration. The resulting energy gain of the ions reaches about 200 MeV, as required in hadron therapy.

4.6 Ion acceleration in near-critical density plasmas

4.6.1 Magnetic vortex acceleration mechanism. There is an advantage of ion acceleration in gas targets — that is, in subcritical density plasmas, where the laser pulse can transfer all its energy to the electrons in a sufficiently thick layer of low-density plasma. Under the conditions of matching the target and laser pulse parameters, the region with a strong electric field can be formed on the rear side of the target [114, 115], where the ion acceleration occurs.

The matching condition corresponds to the equality between the plasma layer thickness $l_{\rm p}$ and the length $l_{\rm dep}$ of the laser pulse energy depletion. The depletion length is equal to the distance through which the laser pulse loses a significant part of its energy, mostly to push the electrons from the self-focusing channel. Taking into account that the characteristic electron energy inside the channel is on the order of $m_{\rm e}c^2a_0$, and invoking the condition of energy balance, we can easily obtain the expression for the depletion length, which has the form

$$l_{\rm dep} = l_{\rm las}\,\frac{n_{\rm c}}{n_{\rm e}}\,a_0\,. \tag{51}$$

Here, $l_{\rm las} = c\tau_{\rm las}$ and a_0 are the length and the normalized amplitude of the laser pulse, respectively.

The amplitude a_0, being known for the laser pulse propagating in a vacuum, may differ significantly inside the plasma because of the relativistic self-focusing of a strong electromagnetic wave [184]. In this case, the power $\mathcal{P} = cE_{\rm las}^2 S/4\pi$ is the key parameter characterizing the laser pulse because, neglecting dissipative processes, it remains constant. Here, S is the cross-section area of the electromagnetic beam. As has been reported in Ref. [185], for a given laser power $\mathcal{P}$ the pulse amplitude inside the self-focusing channel takes the form

$$a_0 = \left(\frac{\mathcal{P}}{\bar{\mathcal{P}}}\,\frac{n_{\rm c}}{n_{\rm e}}\right)^{1/3}. \tag{52}$$

Here, the characteristic power is given by formula $\bar{\mathcal{P}} = 2\kappa m_{\rm e}^2 c^5/e^2 \approx 17.4$ GW, with the coefficient κ equal to unity to an order of magnitude. It is equal to the critical power on the self-focusing threshold at $n_{\rm e} = n_{\rm c}$ [186]. Combining the relationships (51) and (52), we find the optimal regime condition for laser radiation interaction with a plasma target in the form

$$l_{\rm dep} = l_{\rm las}\left(\frac{\mathcal{P}}{\bar{\mathcal{P}}}\right)^{1/3}\left(\frac{n_{\rm c}}{n_{\rm e}}\right)^{4/3}. \tag{53}$$

If the plasma density is such that the target is on the threshold of relativistic transparency, i.e., $n_{\rm e} = n_{\rm c}a_0$, this condition is equivalent to the equality between the thickness of the plasma layer and the length of the laser pulse: $l_{\rm dep} = l_{\rm las}$, which corresponds to several dozen microns for femtosecond lasers.

In the optimal case, the plasma layer thickness and the coordinate of the point at which the laser pulse is focused are chosen so that, on reaching the rear side of the target, the pulse has transferred its energy to the fast electrons. The electric current generated by these electrons is the source of a

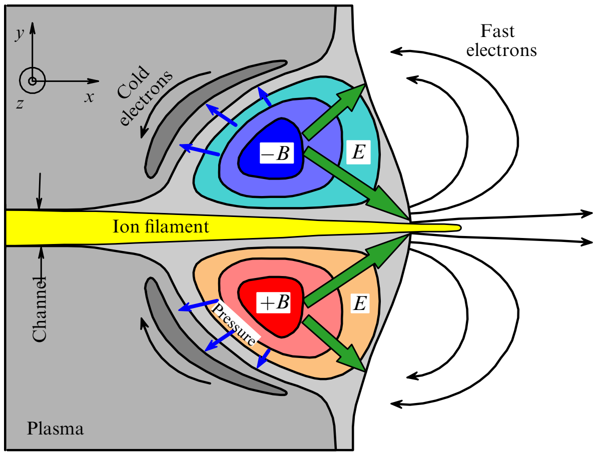

Figure 13. Magnetic and electric field configurations at the target's rear side. The pressure of the toroidal magnetic field leads to the formation of a region with a strong electric field which accelerates and focuses the ions.

quasistatic magnetic field. The magnetic field in laser plasmas can reach values on the order of several hundred megagauss [187, 188].

Due to configuration symmetry, the magnetic field on the target rear side assumes the form of a torus. It plays a dual role here. Under the magnetic field pressure, the electrons are displaced from a certain area, leading to an additional electric charge separation and to an increase in the electric field strength. The resulting electric field has both a longitudinal component, accelerating the positively charged ions, and a radial component, focusing the ion beam. Notice that the magnetic field is here defocusing for positively charged particles. For nonrelativistic ions, the radial force caused by the focusing electric field significantly exceeds the Lorentz force from the magnetic field. In addition, the static magnetic field prevents the return of the electrons to the strong electric field region, thereby preventing it from a charge compensation. Figure 13 illustrates the configurations of the magnetic and electric fields on the target's rear side [105].

The 'magnetic vortex mechanism' of ion acceleration, the theoretical analysis of which has been made in Refs [103–106, 114, 189], was invoked for the interpretation of experiments on laser radiation interaction with various targets, including gas targets [107, 190, 191] and targets comprising a gas–cluster mixture [108]. This mechanism was also applied to explain ion acceleration in the case of solid targets, when, as a result of the finite contrast, the radiation preceding the main pulse evaporated and ionized the solid target, thus turning it into a near-critical density plasma [191– 193].

4.6.2 Ion acceleration at the front of a collisionless shock wave. The fact that ions can be accelerated by collisionless shock waves has been well known since the first publications [194, 195]. In laser plasmas, this ion acceleration mechanism was demonstrated in experiment [196] and was described with PIC computer simulations [197]. Under this ion acceleration scenario, a limited-size region in the plasma target is heated by laser radiation. As a result, a large pressure gradient evolves into the formation of a collisionless ion-acoustic shock wave propagating into the plasma. Due to the charge separation, an electric field is produced at its front. Under this electric field action, part of the plasma ions is reflected from the wave front. Thus, the ions gain energy in the region of electrostatic potential co-moving with the wave. The reflected ions acquire a velocity equal to twice the value of the shock wave velocity. In a plasma with a relatively low initial temperature, the ions reflected by the wave have a narrow energy spectrum, which is of great interest for applications in hadron therapy.

In the experiment [196] mentioned above, in which a 10-TW CO_2 laser interacted with a gas target, a proton beam with an energy of 20 MeV and with a narrow energy spectrum was observed.

In conclusion, following from the discussion in this section, we note that the energy of ions required by hadron therapy can be achieved by using laser systems providing pulses of femtosecond duration and petawatt power. Examples of such laser facilities are given in papers [198, 199].

Along with the requirements of high energy and high quality of accelerated ion beams, it is necessary to ensure the stability of charge particle generation. Emerging technologies, for example, based on synchronized short pulse fiber lasers [200], promise unprecedented stability of the laser parameters from pulse to pulse [201].

5. Formation of high-quality ion beams

For almost all applications of laser accelerators considered in the modern scientific literature, including injectors [202], controlled laser nuclear fusion [203–207], and hadron therapy [35, 208], the quality of the proton beam is of key importance because, if no additional measures are taken, fast protons with a wide energy spectrum are observed in experiments. For this reason, the question arises of how one can provide beams with narrow enough energy distribution, whose width ratio to the characteristic energy, $\Delta\mathcal{E}/\mathcal{E}$, is also small enough. As mentioned in Section 3, ion beams with an energy width of no more than $\Delta\mathcal{E}/\mathcal{E} \leqslant 2 \times 10^{-2}$ are required for the purposes of hadron therapy, which should guarantee a high ratio of the dose in the Bragg peak to the dose at the beam entrance and, accordingly, a sufficiently high dose delivered to the tumor, with an acceptable low dose left in transit healthy tissues.

The development of accelerator technology makes feasible the requirements for the basic parameters of a medical proton beam with the beam intensity of about $(1-5) \times 10^{10}$ protons per second and the maximum energy of 230–250 MeV (see Table. 2). At the same time, applying laser methods of acceleration, it may be difficult to fulfill those other two requirements, which are a relatively small energy spread of the beam, $\Delta\mathcal{E}/\mathcal{E} < 10^{-2}$, and a duty factor of the pulse equal to the actual part of the time of using the bunch, which should not be less than 0.3.

If we compare the energy spectrum shape of the fast ions typically observed in experiments on laser radiation interaction with matter to that required for medical applications, we will see that the currently available ion energy spectrum is far from optimal. From the experiments (see papers [61, 64, 68]), it follows that the energy distribution in the range of energies smaller than the maximal $\mathcal{E}_{\max}$ ($\mathcal{E} < \mathcal{E}_{\max}$) has the quasithermal form, with an efficient temperature several times less than $\mathcal{E}_{\max}$. This spectrum is unacceptable for the medical applications, because it does not provide the optimal shape of the Bragg curve and, consequently, a substantial excess of radiation dose in the target area, which will lead to unacceptably high damage of healthy tissues.

5.1 Selection of a narrow-energy beamlet from the beam with a wide energy spectrum

In order to improve proton beam quality, it is possible to 'cut' it into the beamlets with a narrow energy spectrum. There are many different approaches that use for these purposes achievements in the field of classical charged particle accelerators [209–211], such as magnetic spectrometers, quadrupoles, solenoids, and phase rotators.

5.1.1 Magnetic systems. The energy selector whose concept is explained in Fig. 14a provides an example of a device built around a magnetic system. Used in Refs [47, 48], it is similar to the so-called chickane, known in the field of classical accelerators and free electron lasers. When passing through the region with the magnetic field, due to the fact that ions of different energies have different Larmor radii, the beam is deflected in the direction transverse to its propagation. Then, the beam encounters a screen having a finite width slit. The controlled position and width of the slit determine the energy and the energy spectrum width of the passing ions.

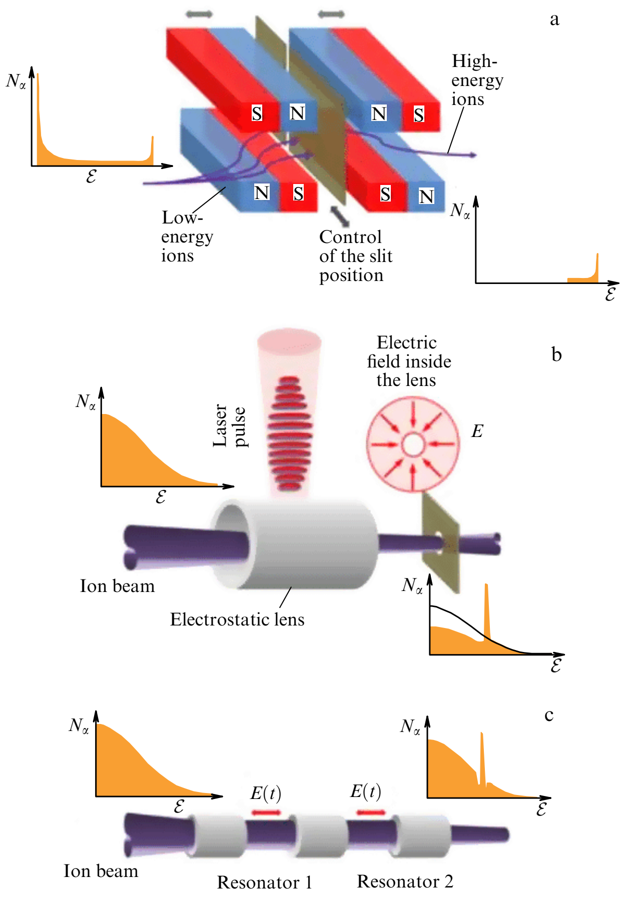

Figure 14. (a) Schematic of the energy selector for forming a narrow-energy spectrum beam from a beam with a wide energy spectrum. Four magnets with alternating sign fields cause ions of different energies to move along different trajectories. Particles with undesirable energy stop at the screen with a slit of finite width, the position and width of which determine the energy and the energy spectrum spread of passing ions. (b) Schematic illustration of an electrostatic lens that focuses an ion beam. The radial electric field inside a thin-wall cylinder is created by electrons accelerated on the outer surface of the cylinder under the action of laser radiation. A similar device was used in Ref. [219]. (c) Principle of operation of a phase rotator. An alternating electric field accelerates (decelerates) the particles forming the beam with the desired energy.

Much attention has also been paid to magnetic quadrupoles used for the purpose of focusing charged particles. The magnetic quadrupole, as is known, is a focusing lens in one direction and a defocusing lens in the other direction. However, a pair of magnetic quadrupoles makes up a focusing lens [211]. In Refs [212, 213], this property was utilized to focus the ion beam generated by laser accelerators.

We also note the theoretical and experimental studies of the quality control of accelerated ion beams with magnetic solenoids [214–217].

5.1.2 Electrostatic systems. As is well known in the optics of charged particle beams [211], electrostatic lenses can also be exploited to focus ions. Since the position of the focus of such lenses depends on the particle energy, these lenses in combination with a screen having an aperture of finite size (small aperture), enable the formation of monoenergetic ion beams.

Quantitatively, the possibility of sharply focusing the charged particle beam is characterized by transverse emittance [209, 210], which is associated with volume conservation in the phase space of the particle system. Emittance is a measure of the beam phase volume. It is equal to the area in the plane r, $r' = \mathrm{d}r/\mathrm{d}x$ occupied by the points of the beam, which is divided by π. Here, r and x are the coordinates transverse and longitudinal with respect to the direction of the beam propagation. The emittance is given by the expression

$$\varepsilon_\perp = \frac{1}{\pi} \oint \mathrm{d}r\,\mathrm{d}r' \,. \tag{54}$$

As an example of ion focusing, let us consider the dynamics of an ion beam in the simplest case of a cylindrical electric lens, in which the electric field is directed radially and is linearly proportional to the coordinate: $E_r = (E_\mathrm{m}/R)r$. The dependence of the beam envelope on the coordinates is described by the equation [209, 210]

$$\frac{\mathrm{d}^2\sigma_r}{\mathrm{d}x^2} + k_\mathrm{b}^2\sigma_r - \frac{\varepsilon_\perp^2}{\sigma_r^3} = 0 \,, \tag{55}$$

where

$$k_\mathrm{b} = \sqrt{\frac{eE_\mathrm{m}}{Rm_\alpha v_x^2}} = \sqrt{\frac{2eE_\mathrm{m}}{R\mathcal{E}_\alpha}} . \tag{56}$$

Here, we neglected the space charge effects, azimuthal asymmetry of the beam, and a change in the particle energy $\mathcal{E}_\alpha$. Introducing the variables $\bar\sigma = \sigma_r/\sqrt{\varepsilon_\perp}$ and $\bar x = k_\mathrm{b}x$, the solution of equation (55) for initial ($\bar x = 0$) values of $\bar\sigma(0) = \bar\sigma_0$ and $\bar\sigma'(0) = \bar\sigma_0'$ can be written out as (see, e.g., Ref. [218])

$$\bar\sigma = \sqrt{\frac{I_0}{2} + \left(\bar\sigma_0^2 - \frac{I_0}{2}\right)\cos(2\bar x) + \bar\sigma_0\bar\sigma_0'\sin(2\bar x)} \,, \tag{57}$$

where the value of I_0 is determined from the boundary condition $I_0 = \bar\sigma_0'^2 + \bar\sigma_0^2 + \bar\sigma_0^{-2}$. Under optimal matching condition implying $\bar\sigma_0' = 0$ and $\bar\sigma_0 = 1$, the ion beam propagates with a constant lateral size. In the case of matching that is not optimal, the beam radius changes between the following values:

$$\bar\sigma_\mathrm{min} = \left(I_0 - \frac{\sqrt{I_0^2 - 4}}{2}\right)^{1/2} \text{ and } \bar\sigma_\mathrm{max} = \left(I_0 + \frac{\sqrt{I_0^2 - 4}}{2}\right)^{1/2} . \tag{58}$$

Due to relationship (56), the position of the focus, viz.

$$\bar x_\mathrm{f} = \frac{1}{2}\arctan\frac{4\bar\sigma_0\bar\sigma_0'}{4\bar\sigma_0 - I_0} \,, \tag{59}$$

depends on the particle energy, which, as noted above, allows using a screen with a small aperture to prepare an ion beam of high quality.

Electrostatic lenses have been realized in experiments [219–222]. In these cases, the electrostatic lens comprised a thin-wall cylinder of a millimeter in diameter (see Fig. 14b). The laser radiation was split into two beams. The first interacted with a thin solid density target, leading to high energy ion generation. The second beam was directed to a cylindrical target, causing an ejection of fast electrons from the inner surface of the target, converging at its axis. As a result, a strong electric field with a radial component was produced inside the cylinder. This electric field focused the accelerated ions. Since the electric field inside the cylinder existed for a finite time interval on the order of 10 ps, it could focus only ions moving at this time inside the electrostatic lens. By changing the delay between the two laser beams, one could monitor energies of ions focused by the lens. In these experiments, an ion beam with an energy of 6 MeV and with a width of the energy spectrum equal to 0.2 MeV was demonstrated.

Ion focusing has also been carried out in a single laser pulse configuration [152, 220]. In later experiments [221], the electrostatic lens was a metal cone a millimeter in size attached to the far side of the target in the path of the propagating laser radiation. The target was irradiated by a laser pulse with an energy of 2 J and with a pulse duration of 60 fs. The accelerated proton beam with an energy of 7 MeV was collimated within a solid angle of about 16 mrad.

Bunching in the energy space of the ions accelerated in the laser plasma was demonstrated in Refs [223–225] with the help of a so-called phase rotator. The principle of operation of the phase rotator, which leads to a change in the distribution of particles in the phase space, is well known in the physics of conventional charged particle accelerators [226]. In this case, an alternating electric field was excited in the RF resonator, as shown in Fig. 14c. Depending on the initial ion velocity and the phase of the alternating electric field, an ion passing through the resonator could gain or lose energy. This has the consequence of increasing or decreasing the number of particles in certain energy intervals and of preparing an ion beam with a narrow energy spectrum.

In all cases, the use of additional devices for manipulating the high-energy ion parameters significantly reduced the conversion efficiency of laser energy into the energy of fast particles, decreased the number of particles of a selected energy in the 'cleansed' beam, and, more importantly, increased the size and cost of the accelerator system; therefore, considerable attention is given to finding alternative solutions.

The main advantage of laser charged particle accelerators is based on the fact that the accelerating electric field and the magnetic field in a laser plasma are many orders of magnitude greater than those of conventional accelerators, provided optimal targets are chosen.

It seems natural to take advantage of these strong electric and magnetic fields in order to control ion beam parameters: the energy spectrum, directionality, and so forth. In Sections 4.1 and 4.2, we pointed out the possibility of generating ion beams with the desired energy spectrum in the Coulomb explosion of clusters and in the target near-surface layer, and the collimation of the beams through the generation of strongly inhomogeneous magnetic fields. Further, we consider a target of a special form for these purposes.

5.2 Special forms of targets

A promising approach to control accelerated ion beams is associated with the ability to implement specially shaped targets. It was proposed in paper [35] to make use of a double-layer target for generating beams with a controllable quality. In this setup, the target consists of two layers: the first of which irradiated by the laser radiation consists of partially ionized heavy ions with charge $Z_\alpha e$ and mass m_α, and the second layer, more distant with respect to the laser beam, consists of lighter ions, e.g., from ionized hydrogen, i.e., protons and electrons. In the initial configuration, the electric charge of positive ions is compensated by the negative charge of the electrons. The number of electrons in the first layer is assumed to be much larger than in the second. The second layer must have a sufficiently small thickness (the dimension along the direction of propagation of the laser pulse) and a sufficiently small width (the size in the transverse direction).

The focusing of accelerated ions is also possible by using targets with a special shape, having the form of a thin-wall concave shell [114, 115, 222, 227, 228] or a thick-wall target with a cavity [229, 230].

Notice that the employment of concave targets for focusing accelerated ions was proposed in Refs [114, 115, 227]. The focusing effect of the ions by such targets has been demonstrated experimentally in Refs [231–234].

5.3 Parameters of a proton beam accelerated in the interaction of laser light with a double-layer target

Under the action of powerful radiation, the target material becomes almost instantaneously ionized. The ionization process is based on an optical mechanism discussed in detail in Refs [235, 236]. As a result, the target is transformed into a thin plasma layer with the above-critical density. Then, the ponderomotive force of the laser radiation pushes the electrons away from the focus area. Since the characteristic time of the hydrodynamic expansion of a micron thick plasma is on the order of nanoseconds, it significantly exceeds the femtosecond laser pulse duration. Under these conditions, the heavy ions remain at rest during the time of pulse exposure to the target. This leads to the formation of a positively charged ion layer with the lateral size on the order of the laser focus. However, after a period of time around the inverse plasma frequency of heavy ions, equal to $1/\omega_{\mathrm{p}\alpha} = \sqrt{m_\alpha/4\pi n_\alpha Z_\alpha e^2}$, where $\omega_{\mathrm{p}\alpha}$ is the plasma frequency of heavy ions, the ion layer starts to expand under the action of Coulomb repulsion of like charges, similar to that discussed above with regard to Coulomb explosion.

If the ratio $\mu^{1/2}/Z_\alpha$, where $\mu = m_\alpha/m_\mathrm{p}$, is large enough, the characteristic time of proton motion is much less than the time of the Coulomb explosion of the heavy ion layer. Under these conditions, the thin proton layer of the double-layer target is accelerated in a given electric field.

For such targets, the smallness of the proton layer width with respect to the lateral size of the laser pulse is one of the most important requirements. The inhomogeneity of the accelerating electric field in the transverse direction, which appears due to the finite width of the laser pulse, leads to additional broadening of the energy spectrum of accelerated ions. The effect of the field transverse inhomogeneity also leads to unwanted defocusing of the ion beam, increasing its transverse emittance. Notice that one of the approaches to mitigate the mentioned effects and to provide high collimation of the ion beam amounts to using targets of a special form (see Ref. [114]).

In order to estimate the characteristic energy of accelerated ions, we assume that all electrons produced in the ionization process in the focus region of the laser beam are ejected from this region under the action of the ponderomotive radiation pressure. In this mode, the electric field in the vicinity of the positively charged layer is $E = 2\pi n_{0\alpha} Z_\alpha e l$. Here, $n_{0\alpha}$ is the ion number density inside the target, and l is the target thickness. The region of the strong electric field localization has a lateral size on the order of the size of the focal area, $R_\perp$. As a result, we can estimate the energy acquired by the proton: $\mathcal{E}_{\max} \approx 2\pi n_{0\alpha} Z_\alpha e^2 l R_\perp$.

We have assumed that the energy of the electrons accelerated in the laser field is greater than or approximately equal to the energy required to overcome the electric field potential attracting them in the acceleration region. Hence, knowing the size of a focal region, $R_\perp$, we can evaluate the required power of the laser pulse, and then, having assigned a pulse duration, find its energy.

The electric field configuration can be approximated by the electrostatic field induced by an oblate charged ellipsoid with a major semiaxis equal to the focal spot size $R_\perp$, and a minor semiaxis (half the thickness) l. The solution giving the electric field of a charged disk can be found in book [72]. Using this solution, we can write the electric field dependence on the coordinates outside of the target:

$$E_x = \frac{4\pi e n_{0\alpha} Z_\alpha l R_\perp^2}{3} \frac{1}{R_\xi} \frac{\partial \xi}{\partial x}\,, \tag{60}$$

$$E_\rho = \frac{4\pi e n_{0\alpha} Z_\alpha l R_\perp^2}{3} \frac{1}{R_\xi} \frac{\partial \xi}{\partial \rho}\,, \tag{61}$$

where x and $\rho = (y^2 + z^2)^{1/2}$ are the polar coordinates, and the function R_ξ and the variable ξ are expressed as

$$R_\xi = (\xi + R_\perp^2)(\xi + l^2)^{1/2}\,, \tag{62}$$

$$\xi = \frac{1}{4}\left\{\left[\left(\rho - \sqrt{R_\perp^2 - l^2}\,\right)^2 + x^2\right]^{1/2} + \left[\left(\rho + \sqrt{R_\perp^2 - l^2}\,\right)^2 + x^2\right]^{1/2}\right\}^2 - R_\perp^2\,. \tag{63}$$

From formulas (60) and (61) follow that the electric field is at its maximum on the target surface and decreases rapidly outside the region on the order of $R_\perp$ in size.

The proton energy spectrum can be found, assuming that the ions move in the paraxial region, which, in turn, corresponds to the structure of our double-layer model. On the axis, the radial component of the electric field vanishes, and the longitudinal component takes the form

$$E_x(x) = \frac{8\pi e n_{0\alpha} Z_\alpha l R_\perp^2}{3} \frac{1}{R_\perp^2 - l^2 + x^2} \,. \tag{64}$$

As is well known, the solution of the kinetic equation for the distribution function $f_{\rm p}(x, v, t)$ can be represented as the relationship

$$f_{\rm p}(x, v, t) = f_{0\rm p}(x_0, v_0) \,, \tag{65}$$

where $f_{0\rm p}(x_0, v_0)$ is the distribution function at the initial instant of time $t = 0$, while $x(t)$ and $v(t)$ are the coordinate and velocity along the particle trajectory (the characteristic) originating at the point (x_0, v_0) in the phase space. We consider the case when, at the initial instant of time, all the particles are at rest and the spatial distribution of their density is given by the function $n_{0\rm p}(x_0)$. These initial conditions are satisfied by the distribution function of the form $f_{0\rm p}(x_0, v_0) = n_{0\rm p}(x_0)\delta(v_0)$, where $\delta(v_0)$ is the Dirac delta function. The number of particles in the unit volume $\mathrm{d}x\,\mathrm{d}v$ of the phase space equals

$$\mathrm{d}n = f_{\rm p}\,\mathrm{d}x\,\mathrm{d}v = f_{\rm p} v\,\mathrm{d}v\,\mathrm{d}t = f_{\rm p}\,\frac{\mathrm{d}\mathcal{E}\,\mathrm{d}t}{m_{\rm p}} \,. \tag{66}$$

This expression integrates over time, yielding the energy spectrum of accelerated particles in the form

$$\mathcal{N}_{\rm p}(\mathcal{E})\,\mathrm{d}\mathcal{E} = \mathrm{d}\mathcal{E} \int n_{0\rm p}(x_0)\delta(v_0)\,\frac{\mathrm{d}t}{m_{\rm p}} = \frac{n_{0\rm p}(x_0)}{m_{\rm p}} \left|\frac{\mathrm{d}t}{\mathrm{d}v}\right|_{v=v_0} \mathrm{d}\mathcal{E} \,. \tag{67}$$

Here, the Lagrange coordinate x_0 and the Jakobian $|\mathrm{d}t/\mathrm{d}v|_{v=v_0}$ are functions of the particle energy $\mathcal{E}$. The coordinate x_0 dependence on energy $\mathcal{E}$ is implicitly defined by the integral of motion

$$\mathcal{E}(x, x_0) = \mathcal{E}_0 + e\big(\varphi(x) - \varphi(x_0)\big) \,, \tag{68}$$

where $\varphi(x)$ is the electrostatic potential. For the electric field given by Eqn (64), one can obtain

$$\varphi(x) = -\frac{4\pi e n_{0\alpha} Z_\alpha l R_\perp^2}{3\sqrt{R_\perp^2 - l^2}} \arctan \frac{\sqrt{R_\perp^2 - l^2}}{x} \,, \tag{69}$$

where x is the particle's running coordinate. In this formulation, we put $\mathcal{E}_0 = 0$ as $x = \infty$. The Jakobian $|\mathrm{d}t/\mathrm{d}v|_{v=v_0}$ is equal to the inverse value of the particle acceleration at the initial instant of time, i.e., $1/|eE(x_0)|$, where the dependence $E(x)$ is given by Eqn (64). On the other hand, the function $1/|eE(x_0)|$ equals $|\mathrm{d}x_0/\mathrm{d}\mathcal{E}|$. Therefore, we obtain the following expression for the energy spectrum of particles:

$$\mathcal{N}_{\rm p}(\mathcal{E})\,\mathrm{d}\mathcal{E} = \left.\frac{n_{0\rm p} x_0}{|\mathrm{d}\mathcal{E}/\mathrm{d}x_0|}\right|_{x_0 = x_0(\mathcal{E})} \mathrm{d}\mathcal{E} \,. \tag{70}$$

It should be noted that this expression for the energy spectrum follows from the general conditions of particle flow continuity in the phase space.

As follows from formula (64), the electric field is locally homogeneous in the near-axis region of the target: $E_x(l) = E = 8\pi e n_{0\alpha} Z_\alpha l/3$. Due to this, the energy spectrum is determined by the form of the dependence $n_{0\rm p}(\varphi^{-1}(\mathcal{E}/e))$.

We see that a unified approach to producing an ion beam with a small energy spectrum width is based on the acceleration of the proton (ion) layers at the initial instant of time, which have a sufficiently small thickness Δx_0. In this case, the energy spread in the proton beam is proportional to the thickness of the layer Δx_0. Characteristic acceleration time is expressed as follows: $t_{\rm acc} = \sqrt{2R_\perp m_{\rm p}/eE_0} \approx \omega_{\rm pp}^{-1}\sqrt{2R_\perp/l}$.

The parameter characterizing the property of the beam to be compressed in the longitudinal direction is the longitudinal emittance $\varepsilon_\parallel$ defined as the product of the energy width $\Delta\mathcal{E}$ and the beam duration Δt. Using the above formulas, we find

$$\varepsilon_\parallel = \Delta\mathcal{E}\Delta t \approx \frac{\Delta x_0}{R_\perp^2} \sqrt{\frac{m_{\rm p}\mathcal{E}R_\perp^2}{2}} \,. \tag{71}$$

For $\Delta\mathcal{E} = 100$ MeV, $\Delta x_0 = 0.1$ μm, and $R_\perp = 1$ μm, the longitudinal emittance is $\varepsilon_\parallel = 2 \times 10^{-2}$ MeV ps.

According to expression (61), the radial electric-field component in the near-axial region close to the target is given by $E_\rho \approx [8\pi e n_{0\alpha} Z_\alpha l^2/(3R_\perp^2)]\,\rho$, i.e., it is a linear function of the radius. From this it follows that the trajectories of the fast particles are described by the formula

$$\rho = \rho_0 \exp\left(\sqrt{kx}\right) \,, \tag{72}$$

where ρ_0 is the initial radial coordinate of a particle, and $k = 2l/R_\perp^2$. As a result, the transverse emittance of the fast proton beam, associated with the transverse nonuniformity of the electric field, at the boundary of the acceleration region, at $x = R_\perp$, is $\varepsilon_\perp = \pi d_0 \theta$. It can be written out as

$$\varepsilon_\perp = \frac{\pi\sqrt{2}\,l d_0}{R_\perp} \,, \tag{73}$$

where d_0 is the lateral size of the proton layer, and the divergence angle of the beam for $kR_\perp \ll 1$ is $\theta \approx \sqrt{2l/R_\perp}$. Thus, for $l \approx d_0 \approx 1$ μm and $R_\perp \approx 5$ μm, the transverse emittance of the beam is about $\varepsilon_\perp \approx 1$ mm mrad.

Energy localization requires that the denominator on the right-hand side of expression (70) be equal to zero at a certain energy $\mathcal{E} = \mathcal{E}_*$, i.e., the Jacobian $|\mathrm{d}\mathcal{E}/\mathrm{d}x_0|$ vanishes. In turn, this indicates that, at the initial instant of time, the accelerated proton layer is localized near the point where the electric field becomes zero. Relationship (70) can be regarded as an equation in function $n_{0\rm p}(x_0)$ for the given energy spectrum and the electric field. Approximating the coordinate dependence of the electric field by the linear function $E(x) = hx$, and the proton number density in a thin layer of thickness L by the function $n_{\rm p}(x) = n_{0\rm p}\theta(L - |x_0|)\theta(x_0)(1 - x_0^2/L^2)$, we obtain the energy spectrum of fast protons in the form

$$\mathcal{N}_{\rm p}(\mathcal{E})\,\mathrm{d}\mathcal{E} = \frac{n_0\,\theta(\mathcal{E} - \mathcal{E}_{\min})\,\theta(\mathcal{E}_{\max} - \mathcal{E})(\mathcal{E} - \mathcal{E}_{\min})}{\Delta\mathcal{E}\sqrt{2eh(\mathcal{E}_{\max} - \mathcal{E})}}\,\mathrm{d}\mathcal{E} \,. \tag{74}$$

Here, the maximum and minimum proton energies are $\mathcal{E}_{\max} = ehR_\perp^2/2$ and $\mathcal{E}_{\min} = eh(R_\perp^2 - L^2)/2$, respectively, i.e., the width of the energy spectrum is $\Delta\mathcal{E} = ehL^2/2$. For a rectangular distribution of the proton number density, $n_{\rm p}(x_0) = n_0\theta(L - x_0)\theta(x_0)$, we obtain a spectrum in the form

$$\mathcal{N}_{\rm p}(\mathcal{E})\,\mathrm{d}\mathcal{E} = \frac{n_0\,\theta(\mathcal{E} - \mathcal{E}_{\min})\,\theta(\mathcal{E}_{\max} - \mathcal{E})}{\sqrt{2eh(\mathcal{E}_{\max} - \mathcal{E})}}\,\mathrm{d}\mathcal{E} \,. \tag{75}$$

As was noted in Section 2.2, such an energy spectrum is desired for tumor irradiation within the framework of the passive dose delivery scenario.

Let us estimate the energy of the protons, which they can acquire in a double-layer target irradiated by a laser pulse of a given power. The realization of the above-discussed acceleration mode requires a laser with high enough intensity I. The electric field of the wave, expressed via its intensity, $E_{\rm las} = \sqrt{4\pi I/c}$, should exceed the field required to remove the electrons from the focus area, i.e., it must be stronger than the characteristic field of the electric charge separation, which, according to Eqn (64), equals $8\pi e Z_\alpha n_{0\alpha} l/3$. Utilizing these relationships and Eqn (69) for the electrostatic potential and assuming that the proton initial coordinate is $x_0 = l$, we obtain the relationship between the proton energy and the laser power $\mathcal{P}_{\rm las} = \pi R_\perp^2 I$. It has the form [97]

$$\mathcal{E}_{\rm p} = \sqrt{\frac{\pi^2 e^2 \mathcal{P}_{\rm las}}{4c}}\,. \tag{76}$$

It is convenient to transform this formula into $\mathcal{E}_{\rm p} = \pi m_{\rm e} c^2 (\mathcal{P}_{\rm las}/\bar{\mathcal{P}})^{1/2}$, where $\bar{\mathcal{P}} = 2m_{\rm e}^2 c^5/e^2 \approx 17.4$ GW [see also Eqn (52)]. Hence, in order to generate protons with an energy of 200 MeV, laser power on the order of 3 PW and an energy of not less than 100 J are required.

5.4 Results of computer simulations of the generation of high-quality proton beams

The discussion in Section 5.3 of the methods for producing proton beams with a small energy spread was based on a simple theoretical model. In order to take into account the numerous nonlinear and kinetic processes that occur in the interaction of high-power laser radiation with a plasma slab, as well as to extend the analysis to two and three dimensions, computer simulations of the protons in the process of a double-layer target irradiation by an ultrashort laser pulse was carried out in Refs [38, 58, 59]. Below, we present the results of three-dimensional simulations.

The simulations were carried out with the REMP (relativistic electromagnetic particle-mesh) code [147]. The simulation region is chosen to have a size of $80\lambda \times 32\lambda \times 32\lambda$, where λ is the wavelength of the laser light. The computational grid has $2560 \times 1024 \times 1024$ cells. The total number of particles varies from 62×10^6 to 820×10^6. The boundaries in the longitudinal direction (along the x-axis) absorb the fields and the particles; in the transverse direction (y, z), the boundary conditions are periodic. It should be noted that the waves coming from the boundaries due to the periodic boundary conditions have a relatively small amplitude and do not impact significantly on the results because of the large transverse dimension of the computational region. The target is modelled with two plasma layers consisting of quasiparticles of three species: electrons, protons, and heavy gold ions. The ratio of the masses of the proton and the electron is $m_{\rm p}/m_{\rm e} = 1836$; for heavy ions, it is $m_\alpha/m_{\rm e} = 195.4 \times 1836/2$.

Initially, the golden foil is localized in the region between the planes with $x = 5.5\lambda$ and $x = 6\lambda$. Its thickness is half a micron, and the diameter is 10 μm, if the wavelength λ of the laser radiation is taken to be 1 μm. A hydrogen layer is deposited on the rear side of the target. It has a thickness of 0.03 μm and a diameter of 5 μm.

The electron concentration inside the heavy-ion layer corresponds to the ratio of the plasma frequency to the frequency of the laser radiation, equal to $\omega_{\rm pe}/\omega = 3$. The second layer is a thin and narrow proton slab (the hydrogen layer can also be contained in a thin plastic layer) located at the initial instant of time at the far side of the target in relation to the laser pulse propagation. Electron concentration inside the proton layer is set to be less than the critical concentration and corresponds to the frequency ratio $\omega_{\rm pe}/\omega = 0.53$.

The collisionless model used here for a target with a given degree of ionization greatly simplifies the problem under consideration, since the implementation of collisions and ionization in the modeling is currently problematic due to the lack of development of the theoretical description of these processes in the limit of petawatt laser radiation powers, and due to the lack of computer resources. We also note that in the regime discussed here, the system evolution depends on the parameter $\int Z_\alpha e n_{0\alpha}\,{\rm d}x \approx Z_\alpha e n_{0\alpha} l$, i.e., on the electric charge surface density in the target. In turn, this means that the same ion acceleration regime in the case of a higher degree of target material ionization may be implemented with a target possessing smaller thickness and higher density.

A laser pulse is initiated at the left boundary of a computational region: $x = 0$. It has a linear polarization with the electric field directed along the z-axis. The dimensionless pulse amplitude is $a_0 = 30$, which corresponds to an intensity of 10^{21} W cm^{-2} for laser radiation with a wavelength of 1 μm. The laser radiation propagates in the x direction. The pulse has the shape of a skewed triangle: its amplitude increases from zero to the maximum value at a front with a length of 3λ, is constant inside the region with the length of 2λ, and linearly decreases to zero in the interval with a length of 10λ. The full diameter of the pulse is equal to 12λ; the amplitude is constant inside a sphere with a diameter of 10λ and decreases to zero at the edges inside the region with a thickness of λ. A fast increase in the radiation amplitude at the pulse front and the absence of both a prepulse and pedestal improves the quality of the accelerated particle beam and can be achieved by using the relativistic transparency effect [180].

The results of computer simulations are presented in Figs 15 and 16. In Fig. 15, the energy spectra of the protons and heavy ions (Fig. 15a) and of electrons (Fig. 15b) at the instant of time $t = 80 \times 2\pi/\omega$ are shown. It is seen that the protons have been accelerated to the energy of about 63 MeV. The relative width of the proton energy spectrum is close to 5%. Heavy ions have a broad energy spectrum with a maximum energy equal to 37 MeV. However, the energy per nucleon is only on the order of 0.2 MeV.

As a result of the double-layer target irradiation by a laser pulse, electrons are ejected predominantly in the radiation propagation direction. Figure 15c depicts the distribution of electric charges within the computational domain. Electrons leaving the target give rise to uncompensated electric charge regions. The light proton layer is accelerated along the x-axis. A layer of heavy ions is expanded as a result of a Coulomb explosion. Ions can be accelerated in this process to an energy corresponding to the value of the electrostatic potential at the initial instant of time. If the electric charge of protons is not compensated, the proton layer can also undergo a Coulomb explosion. In this case, the protons acquire additional kinetic energy due to Coulomb repeling. However, if the total number of protons and their density are relatively small, we can neglect this additional acceleration.

Figure 16 illustrates the angular distribution of the energy of charged particles: protons (Fig. 16a), electrons (Fig. 16b), and heavy ions (Fig. 16c) at $t = 80 \times 2\pi/\omega$. The electron angular distribution is formed by the presence of a beam moving in the wake of a laser pulse and by the isotropic component. The proton layer moves in the direction of laser pulse propagation. The accelerated heavy ions move in the

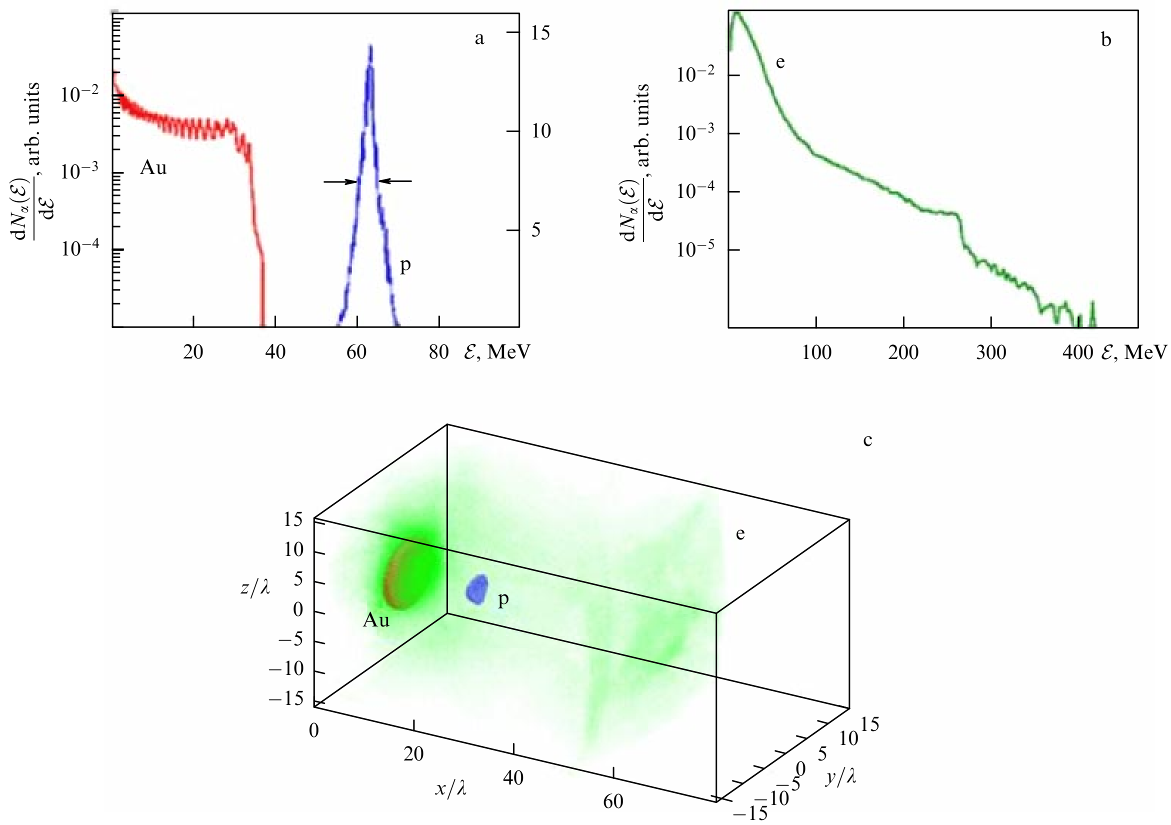

Figure 15. 3D PIC simulation results [58]. Energy spectra of (a) protons and heavy ions, and (b) electrons; (c) distribution of electric charge inside the computational domain at time $t = 80 \times 2\pi/\omega$. Images of electron density (by the ray-tracing method) and of the densities of protons and heavy ions (isosurfaces) are given as an illustration.

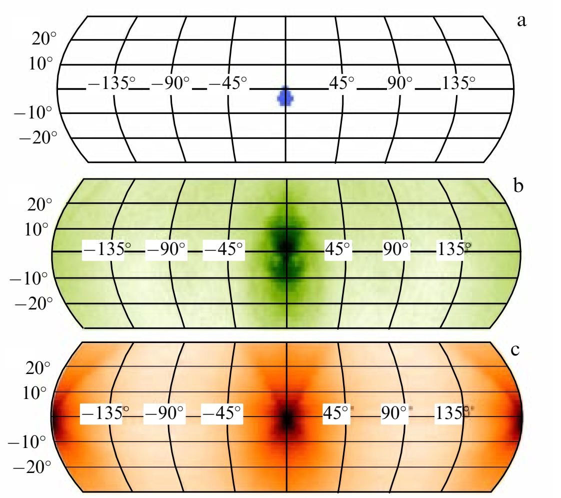

Figure 16. 3D PIC simulation results [58]. The angular distributions of the energies of protons (a), electrons (b), and heavy ions (c) at time $t = 80 \times 2\pi/\omega$. The point $(0°, 0°)$ corresponds to the direction of the laser pulse propagation, and $(0°, 90°)$ is the z-axis direction (direction of the laser radiation polarization).

direction of the laser beam, across and against it, which is characteristic for the Coulomb explosion.

The fact that the highest-energy light ions are concentrated near the axis makes it possible to use a point aperture for selecting a high-quality beam. Namely, a small-size aperture (a small-diameter hole in a thick enough layer of matter) can cut out a portion of the ions with the maximum energies. The smaller the hole diameter, the less the width of the spectrum and the fewer the number of particles in the ion beam prepared.

5.5 Experimental demonstration of laser-accelerated ions with a quasimonoenergetic spectrum

The energy spectrum of fast ions observed in many experiments on the interaction of laser radiation with solid targets shows an exponential type dependence with an effective temperature several times smaller than the maximum energy of ions [237]. However, there are indications of the generation of nonmonotonic ion spectra observed in experiments, e.g., as discussed in Ref. [65]. Figure 7c shows an example of the proton energy distribution obtained by irradiation with a femtosecond laser pulse with the intensity of 5×10^{18} W cm^{-2} of an aluminum foil with a thickness of 12.5 μm. The angle of incidence of the laser radiation onto the target is equal to 45°. In this case, the source of protons comprised a thin water film on the surface of the target. Nonmonotonous energy dependence could be accounted for, for example, by a specific form of the electron distribution function [see Eqns (25) and (26)].

The approaches in which it is possible to control such parameters of ion beams as their composition, energy spectrum, angular distribution, etc., are of paramount importance for applications. The paradigm theoretically formulated in Ref. [35] and covering the employment of double-layer targets for controling the quality of accelerated ions was a motivation for the experiments, the results of which were reported in Refs [60, 238].

A titanium target with a thickness of 5 μm was prepared for these experiments. The plastic structure (it is an organic

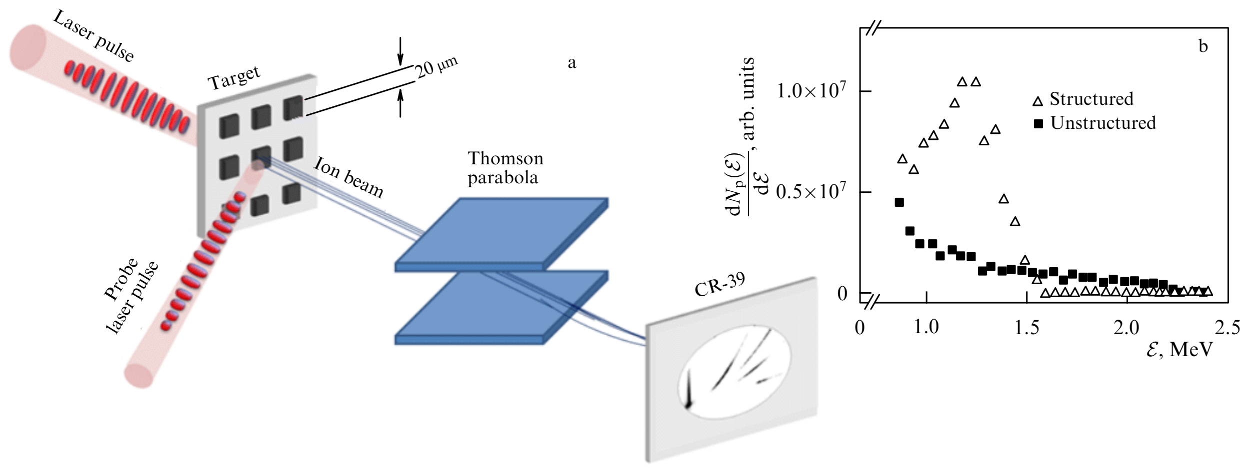

Figure 17. (a) Setup of experiment [60]. The high-power laser pulse is incident on the structured target at an angle of 45°. The low-power probe pulse is used to align the position of the focal region and the plastic spots on the target far side. Ions of different energies are bent in space using a Thomson parabola and are registered by CR-39 films or microchannel plates. A detailed description of the detectors of fast ions can be found in reviews [64, 68]. (b) Energy spectrum of protons from a structured target (triangles) and a target without a microstructure (squares) [60].

glass — polymethylmethacrylate) is applied on the target's rear side as shown in Fig. 17. The titanium layer is a source of heavy ions. Hydrogenous plastic spots play the role of a second thin and narrow source of light ions. The characteristic size of the plastic patches is $20 \times 20 \times 0.5$ μm^3.

The microstructured target is irradiated by the laser pulse with a radiation intensity of 3×10^{19} W cm^{-2}. The pulse duration is equal to 80 fs. A second, weaker laser pulse is used to align the position of the focal region and the plastic spots on the far side of the target. Accelerated protons propagate in the direction normal to the target surface. Particles are registered by the detector consisting of a Thomson parabola and CR-39 films or microchannel plates.

Figure 17b displays the proton energy spectra for microstructured and nonstructured targets. In the latter case, the accelerated protons originate from a thin water layer on the target surface. In the energy range from 0.5 to 2.5 MeV, the distribution of the protons with the full number of particles in the solid angle of 24 msr equals 10^8. The ion spectrum generated by microstructured targets has a maximum at an energy of 1.2 MeV and a width of about 25%. In targets without a microstructure, the proton energy spectrum can be approximated by an exponential function.

It should be noted that the use of microstructured targets can increase the efficiency of ion acceleration [239, 240]. In this approach, patterns with a characteristic size of about 1 μm, which is commensurate with the wavelength of laser radiation, are imposed on the front target side relative to the laser pulse propagation direction. Under the matching conditions, which also depend on the angle of the electromagnetic wave incidence on the target and on the radiation polarization, the radiation absorption is higher. This, in turn, leads to the generation of a larger number of high-energy electrons and an increase in the energy and number of accelerated ions.

5.6 Optimization of targets and laser pulses for achieving ion parameters required in hadron therapy

Theoretical and experimental studies of laser ion acceleration have been constantly focused on revealing the optimal regimes [132, 241, 242]. The goal of such studies is to formulate recommendations on how to choose the target parameters for achieving the maximum energy and number of accelerated ions at realistic values of the energy and power of the laser pulses.

In regard to enhancing the ion acceleration efficiency, so-called mass-limited targets have certain advantages. A typical example of such a target is a double-layer target. Due to the limited size of such targets, the fast electrons cannot leave the laser focus region in the process of their irradiation by laser radiation of moderate power insufficient for the implementation of the regime of Coulomb explosion. This occurs in contrast to targets of a larger size, in which fast electrons are replaced by cold electrons coming from the periphery of the target, thus compensating the electric charge. For this reason, the electric field of charge separation in the mass-limited targets exists for a relatively long time. In turn, this leads to the acceleration of the higher number of ions.

According to Ref. [243], the exploitation of the mass-limited targets can enhance the proton acceleration efficiency twofold over a wide target of the same thickness.

PIC simulations of the ion acceleration in a three-dimensional geometry, presented in Ref. [241], showed that protons with the energy of 200 MeV can be obtained by irradiating the double-layer target with a laser pulse having a power of 0.7 PW, energy of 20 J, and intensity of 5×10^{21} W cm^{-2}.

An important factor of ion acceleration optimization, as noted in Section 4, is the involvement of a laser prepulse, which leads to the formation of a plasma corona on the front side of the target. As follows from multiparametric computer simulations [132], too strong a prepulse creates an extended plasma corona which absorbs the main pulse. Although a significant portion of the main pulse energy is transferred to the fast electrons, which generates an electric field on the target's rear side, the acceleration of ions occurs in a nonoptimal regime. This is because the high-energy electrons, having a wide angular distribution in momentum space and a low number density, create a relatively weak electric field. The situation is radically different if the size of the plasma corona is commensurable with the length of the laser pulse, i.e., is approximately several dozen microns. In this case, on the one hand, the intensity of the laser pulse increases significantly due to relativistic self-focusing. On the other hand, the laser pulse can penetrate to the interior of the solid target. In this case, the ion acceleration happens as a result of several consecutive steps, starting from the acceleration in the near-surface layer of the target, followed by directed Coulomb explosion and radiation pressure acceleration.

The direction of the beam of accelerated ions can be controlled by changing the angle of incidence of the laser radiation on the target [244]. In this way, it is possible to scan a tumor within the active dose delivery scenario.

6. Radiobiological effectiveness of beams of protons accelerated in laser plasmas

In the vast majority of theoretical and experimental work devoted to studying ion acceleration in laser plasmas, which were published in the last 10 years, hadron therapy of cancer has been indicated as one of the most important applications. From here naturally follows the question about the relative biological effectiveness of high-energy ions accelerated by laser radiation, in comparison with ions generated by conventional accelerators. First of all, such a distinction, if it exists, may be due to the very short duration of the laser-accelerated ion beams. Because of this, the high instantaneous intensity of the ion beam is many orders of magnitude larger than the intensity of ion beams accelerated by conventional accelerators. There are indications that, in the high-intensity interaction of fast ions with DNA molecules, clusters can be formed, which may increase the probability of the double strand break and, accordingly, increase the probability of killing the cancer cells [13, 22]. From the point of view of experiments on cancer cell irradiation by protons accelerated in laser plasmas, it should be seen in the dependence of the number of survived cells on the dose and in the dependence of the relative biological effectiveness on the linear energy transfer, as well as on the duration of the beam pulse. Papers [47–54] are devoted to the study of these problems.

The first publications devoted to this problem [47] reported the results of exposure of live cancer cells to protons accelerated in a laser plasma.

The experiment schematic is presented in Fig. 18. Ions are generated by one of the mechanisms described in Section 4 in the process of laser radiation interaction with the target. The

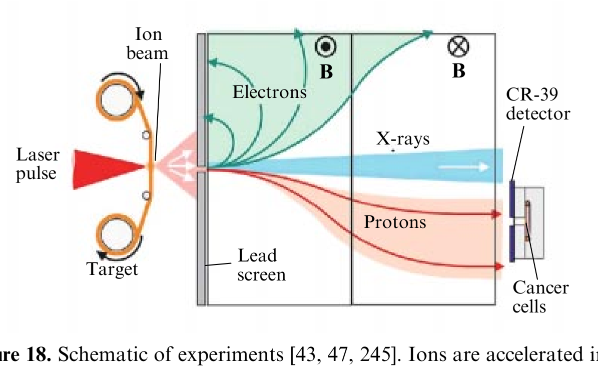

Figure 18. Schematic of experiments [43, 47, 245]. Ions are accelerated in the process of laser radiation interaction with a thin foil target, which is similar to the tape pulled in a magnetic recorder. The fast ions, electrons, and X-rays passing through the collimator enter the magnetic selector in which the ion trajectories are separated from the electron and X-ray trajectories. The ion beam with the required energy is selected by the second small-aperture collimator. The resulting beam irradiates living cancer cells contained in a special container.

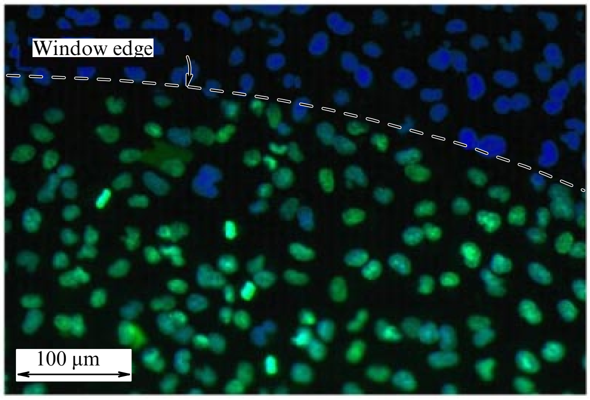

Figure 19. γ-H2AX centers generated by the irradiation of cancer cells with the proton beam delivering the dose of 20 Gy [46]. Cells with double strand breaks of DNA stained with the aid of 4′,6-diamino-2-phenylindole (DAPI) used in fluorescence microscopy.

target is a thin foil pulled like the tape in a magnetic recorder. Fast ions with electrons accompanying them and X-rays enter the magnetic selector through the first collimator in a lead screen, where the trajectories of ions are deflected according to their energies. The electrons are deflected in the opposite direction. Since X-ray photons do not interact with the magnetic field, they propagate along straight trajectories. The second small-aperture collimator selects the ion beam with the required energy. This beam then enters the capsule where it irradiates the culture of cancer cells. The fact that the positively charged ions, negatively charged electrons, and chargeless photons propagate along different trajectories makes attractive the application of such a magnetic system for preventing unwanted exposure of the target to radioactive debris — that is, to electrons, neutrons, photons, neutral atoms and molecules, and so on.

In the experiment discussed, cell irradiation was performed *in vitro*. A549 cancer cells of the lung, adenocarcinoma were irradiated by a quasimonoenergetic proton beam with an energy in the range from 0.8 to 2.4 MeV. The proton energy spectrum is formed with the aid of the energy selector described above (see Figs 14, 18 and Ref. [246]). The bunch has a duration of 1.5×10^{-8} s. The particle flux amounts to $\approx 10^{15}$ cm^{-2} s^{-1}. The delivered beam dose is 20 Gy. As a result, the γ-H2AX type centers are formed, as is clearly seen in Fig. 19. They are unambiguous indicators of the double strand break in the DNA molecules of cancer cells. Without dwelling on the details of the method outlined in Ref. [247], we note that they used a property of histone staining in the cell with DNA undergoing the double strand breaking.

The results of similar experiments, when cancer cells taken from tumors of the salivary gland have been irradiated *in vitro*, are presented in Ref. [48]. A proton beam with a narrow energy spectrum width of 0.66 MeV near the energy of 2.25 MeV had a pulse duration of 20 ns. The percentage of cells that survived the irradiation with a total dose of order 8 Gy was measured. For the exposure rate in a single proton beam pulse equal to 1×10^7 Gy s^{-1}, the effective exposure rate corresponded to 0.2 Gy s^{-1} for the laser repetition rate of 1 Hz.

With the dose increasing, the portion of surviving cells decreases, as follows from the dependence presented in Fig. 20a. This figure shows the dependence of the fraction of

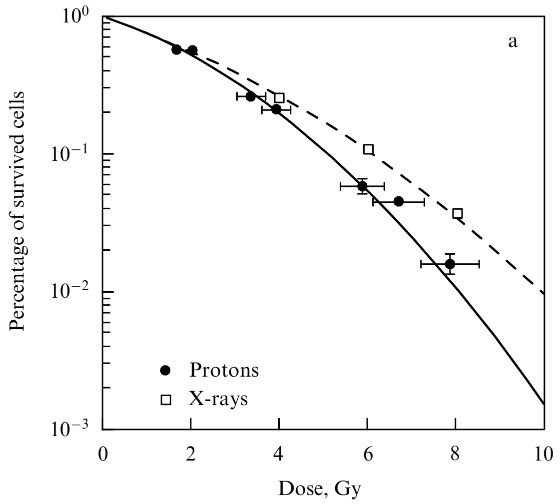

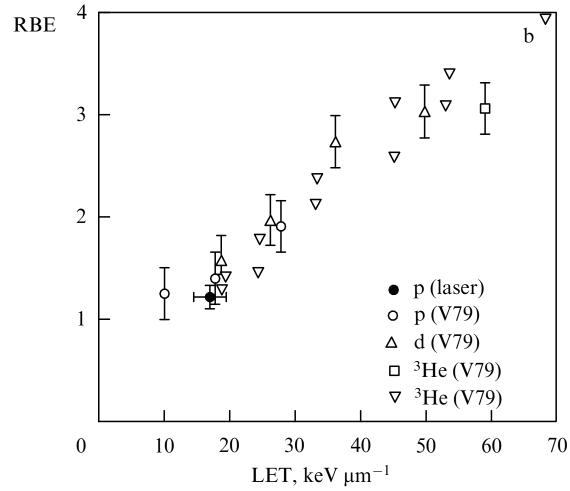

Figure 20. (a) Percentage of survived cells depending on the irradiation dose during cancer cell irradiation by protons accelerated in a laser plasma. For comparison, a similar dependence is shown for the case of X-ray irradiation [48]. (b) Dependence of the relative biological effectiveness (RBE) on the linear energy transfer (LET) for protons and ions obtained using conventional accelerators [248, 249] and accelerated in the laser plasma [245].

survived cells on the exposure dose during cancer cell irradiation by protons accelerated in the laser plasma. For comparison, we also depict the dependence corresponding to X-ray irradiation. Solid and dashed lines correspond to the approximation within the framework of linear-quadratic models [250]. In this model, the dependence of the fraction of survived cells on the dose is given by expression (2). For protons, the data in Fig. 20b give $\alpha = 0.243 \pm 0.027$ and $\beta = 0.0409 \pm 0.0091$.

Measured relative biological effectiveness $(D_{\rm p}/D_{\gamma})$, defined by Eqn (1), for the 10% fraction of survived cells is equal to 1.20 ± 0.11. Under the experiment's conditions, the LET, the linear energy transfer, equals 17.1 keV μm^{-1}. Note that in experiments [248] on cancer cell irradiation by protons accelerated with standard accelerators, the value of $\text{RBE} = 1.20 \pm 0.11$ was obtained for the particles with $\text{LTE} = 17.1 \pm 2.8$ keV μm^{-1}, which is very close to the values corresponding to ions accelerated by classical accelerators. For comparison, we show in Fig. 20b the dependence of the RBE on the LET in the cases of cancer cell exposure to light ions generated by conventional accelerators, and to protons accelerated in the process of interaction of powerful laser radiation with solid targets.

Encouraging results obtained in the experiments discussed above give no reason to think that the RBE of ultrashort pulsed ion bunches with the same LET and with other equal parameters are markedly different from the RBE for continuous ion beams and beams with the traditionally used duration from fractions of a second to several seconds.

7. Conclusions

Radiation therapy gives an impressive example of the medical applications of the results obtained in fundamental and applied physics, starting from discovery of the X-rays, the development of particle accelerators, and concluding with the establishment of methods for computer tomography and nuclear magnetic resonance (see, for example, the discussion in Ref. [251]). The development of technologies enabling fabrication of relatively small-size powerful lasers and progress in the physics of collective methods of charged particle acceleration in plasma, as expected, will lead to the creation of a compact medical ion accelerator.

Ions with energies above the average thermal limit have been detected in experiments on the interaction of laser radiation with different targets, starting in the 1960s [252, 253]. The acceleration of ions at the front of a plasma cloud expanding into a vacuum was considered at that time as the main acceleration mechanism [157–163]. By the end of the 1990s, the development of laser technology had reached the level that allowed obtaining directed high-energy ion beams in experiments on the irradiation of thin foils [254–256]. Progress in the experimental physics of strong laser fields has been accompanied by the development of adequate theoretical models supported by computer simulations. This led in the late 1990s and the early 2000s to the formulation and substantiation of a wide range of applications of laser ion accelerators, including various problems of nuclear medical physics [63, 257, 258], where the the central place is occupied by hadron therapy of cancers.

Papers [35, 38, 259, 260] formulate a concept in which, in its minimum version, a laser ion accelerator replaces the standard accelerator (or even the injector), while systems of ion delivery and target irradiation remain unchanged, e.g., as described in Ref. [42]. In its highest, most promising version, traditional accelerators and magnetic systems of ion beam delivery and control are completely removed and replaced by an all-optical system. On the way towards this promising version, it is necessary to solve a number of sophisticated technical problems, among which especially important is the enhancement of laser pulse stability and repetition rate, in connection with an increase in average laser power.

At the intermediate stage of medical laser accelerator development, electromagnetic devices providing control of the appropriate ion beam quality seem to be required.

In the paradigm of active dose delivery to the tumor, subsystems of beam delivery and target scanning make a carefully adjusted integrated complex together with the accelerator of charged particles. In addition, since the independent optimization of individual components is not sufficient for achieving the required efficiency, the synchronous and coherent parameter control of all the components is necessary, starting from the ion source and concluding with the scanning device. Similarly, a laser ion source being integrated into a single complex must be controllable by the systems ensuring the correspondence of laser parameters to the therapeutic plan, including dose monitoring. The integration, in particular, implies the real-time control of such ion beam parameters as the energy spectrum, the number of particles in the beam, and their propagation direction. In this regard, the laser ion accelerator has great advantages that should be fully realized. Therefore, the situation considered in many articles, when the laser accelerator is inserted into an existing therapeutic system, only replacing a medical cyclotron or synchrotron, is obviously far from being optimal.

We note here that the process of scanning by an ion beam can be easily realized by tilting the target or by changing the angle of laser beam incidence with respect to the target. In this case, the direction of the accelerated ion beam deflects from the target normal due to relativistic effects, as determined by a regular dependence (see a detailed discussion of this issue in Refs [244, 261, 262]).

As noted above, the main advantage of laser particle accelerators stems from the fact that the accelerating electromagnetic field generated in laser plasmas is many orders of magnitude greater than that in conventional accelerators. For this reason, it is natural to use this strong electromagnetic field for controling the ion beam parameters by virtue of targets of a special form.

The area of potential applications of laser accelerators of high-energy ions is not confined to hadron therapy. As in the case of conventional accelerators, it is necessary to bear in mind the above-mentioned problems of space medicine [23] and the application of ion beams to the treatment of nononcological diseases [263], including radiosurgery [264]. In regard to the latter, it is worth paying attention to the prospect of the development of a highly efficient ultrahigh-power laser source of gamma-rays [265–267].

Since the development of high-power laser technology requires significant investments, there is a selection of objectives and areas based on the criteria of their feasibility and the demands for them. Certainly, this also concerns laser medical accelerators. Nevertheless, the expected social benefit of laser accelerator implementation in cancer therapy is so great that practically all scientific groups working on the development of laser methods of charged particle acceleration formulate in their research programs ion acceleration for hadron therapy as one of the central goals.

Acknowledgments

The authors are grateful to A A Andreev, M Borghesi, V Yu Bychenkov, S Yu Gus'kov, H Daido, E Yu Echkina, T M Jeong, A G Zhidkov, W Sandner, I N Inovenkov, A Yogo, S Kawata, M Kando, S Kar, Y Kato, H Kiriyama, G I Klenov, J Koga, K Kondo, W P Leemans, J Limpouch, C-M Ma, A Maximchuk, D Margarone, K Mima, T Morita, M Murakami, G A Mourou, C Nam, P Nickles, D Niley, M Nishiuchi, K Nishihara, A Noda, K Ogura, F Pegoraro, M Roth, J Rydki, S Sakabe, Y Sentoku, V Scuderi, A N Starostin, T Tajima, S Ter-Avetisyan, Y Fukuda, A Zigler, G A P Cirrone, and W T Chu for many helpful discussions. One of the authors (S V B) expresses appreciation to the Institute of Physics of the Czech Academy of Sciences and ELI-Beamlines for their support of this work.

References

1. Lodish H et al. *Molecular Cell Biology* 5th ed. (New York: W.H. Freeman, 2003)
2. Dokukin M E et al. *Phys. Rev. Lett.* **107** 028101 (2011)
3. Goitein M, Lomax A J, Pedroni E S *Phys. Today* **55** (9) 45 (2002)
4. Gol'din L L et al. *Sov. Phys. Usp.* **16** 402 (1973); *Usp. Fiz. Nauk* **110** 77 (1973)
5. Chu W T, Ludewigt B A, Renner T R *Rev. Sci. Instrum.* **64** 2055 (1993)
6. Khoroshkov V S, Minakova E I *Eur. J. Phys.* **19** 523 (1998)
7. Kraft G *Prog. Part. Nucl. Phys.* **45** 473 (2000)
8. Kraft G *Physica Medica* **17** (Suppl. 1) 13 (2001)
9. Amaldi U *Physica Medica* **17** (Suppl. 1) 33 (2001)
10. Regler M et al. "Medical accelerators for hadrontherapy with protons and carbon ions (with an introduction to the physical advantage of heavy-charged particle radiation)", in *CERN Accelerator School*: *Intermediate Accelerator Physics, Seville, Spain, October 15–26, 2001* (Hephy-PUB-757/02)
11. Khoroshkov V S *Phys. Atom. Nucl.* **69** 1724 (2006); *Yad. Fiz.* **69** 1760 (2006)
12. Fortov V E, Hoffmann D H H, Sharkov B Yu *Phys. Usp.* **51** 109 (2008); *Usp. Fiz. Nauk* **178** 113 (2008)
13. Schardt D, Elsässer T, Schulz-Ertner D *Rev. Mod. Phys.* **82** 383 (2010)
14. Durante M, Loeffler J S *Nature Rev. Clin. Oncol.* **7** 37 (2010)
15. Newhauser W D, Durante M *Nature Rev. Cancer* **11** 438 (2011)
16. Miralbell R et al. *Int. J. Radiat. Oncol. Biol. Phys.* **54** 824 (2002)
17. Moteabbed M, Yock T, Paganetti H *Phys. Med. Biol.* **59** 2883 (2014)
18. Puck T T *Sci. Am.* **202** (4) 142 (1960)
19. Khoroshkov V S, in *Trudy XVIII Mezhdunarodnoi Konf. "Novye Informatsionnye Tekhnologii v Meditsine, Biologii, Farmakologii i Ekologii", Gurzuf, 2010* (Proc. of the XVIII Intern. Conf."New Information Technologies in Medicine, Biology, Pharmacology and Ecology," Gurzuf, 2010) p. 40
20. Boudaïffa B et al. *Science* **287** 1658 (2000)
21. Boudaïffa B et al. *Radiat. Res.* **157** 227 (2002)
22. Blakely E A, Kronenberg A *Radiat. Res.* **150** S126 (1998)
23. Durante M, Cucinotta F A *Rev. Mod. Phys.* **83** 1245 (2011)
24. Kobayashi Y et al. *Nucl. Instrum. Meth. Phys. Res. B* **210** 308 (2003)
25. Dollinger G et al. *Nucl. Instrum. Meth. Phys. Res. B* **231** 195 (2005)
26. Folkard M et al. *J. Phys. B At. Mol. Opt. Phys.* **32** 2753 (1999)
27. Denifl S et al. *Int. J. Mass Spectrometry* **232** 99 (2004)
28. Wilson R R *Radiology* **47** 487 (1946)
29. Bragg W H, Kleeman R *Philos. Mag.* **10** 318 (1905)
30. http://ptcog.web.psi.ch/ptcentres.html
31. Schulz-Ertner D, Tsujii H *J. Clin. Oncol.* **25** 953 (2007)
32. Debus J, Kraft G, Hug E "Hadronentherapie", in Bamberg M, Molls M, Sack H (Hrsg.) *Radioonkologie* Bd. 1 *Grundlagen* (München: W. Zuckschwerdt, 2009) p. 95
33. Caporaso G J et al. *Phys. Med.* **24** 98 (2008)
34. Schippers J M, Lomax A J *Acta Oncol.* **50** 838 (2011)
35. Bulanov S V, Khoroshkov V S *Plasma Phys. Rep.* **28** 453 (2002); *Fiz. Plazmy* **28** 493 (2002)
36. Tajima T *J. Jpn. Soc. Therap. Rad. Oncol.* **9** 83 (1989)
37. Ma C-M et al. *Med. Phys.* **28** 868 (2001)
38. Bulanov S V et al. *Phys. Lett. A* **299** 240 (2002)
39. Fourkal E et al. *Med. Phys.* **29** 2788 (2002)
40. Malka V et al. *Med. Phys.* **31** 1587 (2004)
41. Tajima T et al. *Rev. Accel. Sci. Technol.* **2** 201 (2009)
42. Bolton P R et al. *Nucl. Instrum. Meth. Phys. Res. A* **620** 71 (2010)
43. Murakami M et al. *AIP Conf. Proc.* **1024** 275 (2008)
44. Mourou G A et al. (Eds) *ELI — Extreme Light Infrastructure Science and Technology with Ultra-Intense Lasers WHITEBOOK* (Berlin: THOSS Media GmbH, 2011)
45. Cirrone G A P et al. *Proc. SPIE* **8779** 87791I (2013)
46. Schell S, Wilkens J J *Med. Phys.* **37** 5330 (2010)
47. Yogo A et al. *Appl. Phys. Lett.* **94** 181502 (2009)
48. Yogo A et al. *Appl. Phys. Lett.* **98** 053701 (2011)
49. Kraft S D et al. *New J. Phys.* **12** 085003 (2010)
50. Bin J et al. *Appl. Phys. Lett.* **101** 243701 (2012)
51. Doria D et al. *AIP Adv.* **2** 011209 (2012)
52. Richter R et al. *Phys. Med. Biol.* **56** 1529 (2011)

53. Zeil K et al. *Appl. Phys. B* **110** 437 (2013)
54. Kar S et al. *AIP Conf. Proc.* **1546** 87 (2013)
55. Linz U, Alonso J *Phys. Rev. ST Accel. Beams* **10** 094801 (2007)
56. Schulz R J, Kagan A R *Med. Phys.* **30** 276 (2003)
57. Nyström H *Acta Oncol.* **49** 1124 (2010)
58. Esirkepov T Zh et al. *Phys. Rev. Lett.* **89** 175003 (2002)
59. Bulanov S V et al. *Plasma Phys. Rep.* **28** 975 (2002); *Fiz. Plazmy* **28** 1059 (2002)
60. Schwoerer H et al. *Nature* **439** 445 (2006)
61. Borghesi M et al. *Fusion Sci. Technol.* **49** 412 (2006)
62. Mourou G A, Tajima T, Bulanov S V *Rev. Mod. Phys.* **78** 309 (2006)
63. Ledingham K W D, Galster W *New J. Phys.* **12** 045005 (2010)
64. Daido H, Nishiuchi M, Pirozhkov A S *Rep. Prog. Phys.* **75** 056401 (2012)
65. Maksimchuk A et al. *Plasma Phys. Rep.* **30** 473 (2004); *Fiz. Plazmy* **30** 514 (2004)
66. Belyaev V S et al. *Phys. Usp.* **51** 793 (2008); *Usp. Fiz. Nauk* **178** 823 (2008)
67. Tikhonchuk V T *Nucl. Instrum. Meth. Phys. Res. A* **620** 1 (2010)
68. Macchi A, Borghesi M, Passoni M *Rev. Mod. Phys.* **85** 751 (2013)
69. Kraft G, in *Advances in Hadrontherapy*: *Proc. of the Intern. Week on Hadrontherapy, European Scientific Institute, Archamps, France, 20 – 24 November 1995 and of the Second Intern. Symp. on Hadrontherapy, PSI, and CERN, Switzerland, 9 – 13 September 1996* (International Congress Series, Vol. 1144, Eds U Amaldi, B Larsson, Y Lemoigne) (Amsterdam: Elsevier, 1997) p. 385
70. Elsässer Th et al. *Int. J. Radiat. Oncol. Biol. Phys.* **78** 1177 (2010)
71. Weber U, Kraft G *Cancer J.* **15** 325 (2009)
72. Landau L D, Lifshitz E M *Electrodynamics of Continuous Media* (Oxford: Pergamon Press, 1984); Translated from Russian: *Elektrodinamika Sploshnykh Sred* (Moscow: Nauka, 1982)
73. Fortov V E, Sharkov B Yu, Stöcker H *Phys. Usp.* **55** 582 (2012); *Usp. Fiz. Nauk* **182** 621 (2012)
74. Fano U *Annu. Rev. Nucl. Sci.* **13** 1 (1963)
75. Highland V L *Nucl. Instrum. Meth.* **129** 497 (1975)
76. Hishikawa Y et al. *Int. J. Radiat. Oncol. Biol. Phys.* **53** 1388 (2002)
77. Enghardt W et al. *Nucl. Instrum. Meth. Phys. Res. A* **525** 284 (2004)
78. Parodi K et al. *Int. J. Radiat. Oncol. Biol. Phys.* **68** 920 (2007)
79. Korzhimanov A V et al. *Phys. Usp.* **54** 9 (2011); *Usp. Fiz. Nauk* **181** 9 (2011); *Phys. Rev. Lett.* **109** 245008 (2012)
80. Nishiuchi M et al. *Rev. Sci. Instrum.* **85** 02B904 (2014)
81. Min C-H et al. *Appl. Phys. Lett.* **89** 183517 (2006)
82. Verburg J V et al. *Phys. Med. Biol.* **58** L37 (2013)
83. Knopf A C, Lomax A *Phys. Med. Biol.* **58** R131 (2013)
84. Bauer S et al. *Phys. Med. Biol.* **58** R97 (2013)
85. Iwase H et al. *J. Nucl. Sci. Technol.* **39** 1142 (2002)
86. Kraft G (for the Heavy Ion Therapy Collab.) *Nucl. Instrum. Meth. Phys. Res. A* **454** 1 (2000)
87. Pedroni E et al. *Med. Phys.* **22** 37 (1995)
88. Haberer Th et al. *Nucl. Instrum. Meth. Phys. Res. A* **330** 296 (1993)
89. Furukawa T et al. *Med. Phys.* **37** 4874 (2010)
90. Bulanov S V et al., in *Reviews of Plasma Physics* Vol. 22 (Ed. V D Shafranov) (New York: Kluwer Acad./Plenum Publ., 2001) p. 227
91. Ogura K et al. *Opt. Lett.* **37** 2868 (2012)
92. Kim I J et al. *Phys. Rev. Lett.* **111** 165003 (2013)
93. Jeong T M, private communication
94. Jung D et al. *Phys. Plasmas* **20** 083103 (2013)
95. Hegelish B M et al., arXiv:1310.8650
96. Wilks S C et al. *Phys. Plasmas* **8** 542 (2001)
97. Bulanov S V et al. *AIP Conf. Proc.* **740** 414 (2004)
98. Esirkepov T et al. *Phys. Rev. Lett.* **92** 175003 (2004)
99. Klimo O et al. *Phys. Rev. ST Accel. Beams* **11** 031301 (2008)
100. Liu J-L et al. *Phys. Plasmas* **20** 063107 (2013)
101. Bulanov S V et al. *Comptes Rendus Phys.* **10** 216 (2009)
102. Echkina E Yu et al. *Plasma Phys. Rep.* **36** 15 (2010); *Fiz. Plazmy* **36** 17 (2010)
103. Kuznetsov A V et al. *Plasma Phys. Rep.* **27** 211 (2001); *Fiz. Plazmy* **27** 225 (2001)
104. Bulanov S V et al. *Plasma Phys. Rep.* **31** 369 (2005); *Fiz. Plazmy* **31** 409 (2005)
105. Bulanov S V, Esirkepov T Zh *Phys. Rev. Lett.* **98** 049503 (2007)
106. Nakamura T et al. *Phys. Rev. Lett.* **105** 135002 (2010)
107. Willingale L et al. *Phys. Rev. Lett.* **96** 245002 (2006)
108. Fukuda Y et al. *Phys. Rev. Lett.* **103** 165002 (2009)
109. Chu W T et al., Report of the Advisory Group Meeting. F1-AG-1010, IAEA Headquarters, Vienna, 7 – 10 July 1998
110. Weber U, Becher W, Kraft G *Phys. Med. Biol.* **45** 3627 (2000)
111. Denavit J *Phys. Rev. Lett.* **69** 3052 (1992)
112. Lawson W S, Rambo P W, Larson D J *Phys. Plasmas* **4** 788 (1997)
113. Esirkepov T Zh et al. *JETP Lett.* **70** 82 (1999); *Pis'ma Zh. Eksp. Teor. Fiz.* **70** 80 (1999)
114. Bulanov S V et al. *JETP Lett.* **71** 407 (2000); *Pis'ma Zh. Eksp. Teor. Fiz.* **71** 593 (2000)
115. Sentoku Y et al. *Phys. Rev. E* **62** 7271 (2000)
116. Esarey E, Schroeder C B, Leemans W P *Rev. Mod. Phys.* **81** 1229 (2009)
117. Bulanov S V et al. *Plasma Phys. Rep.* **30** 18 (2004); *Fiz. Plazmy* **30** 21 (2004)
118. Peano F et al. *New J. Phys.* **10** 033028 (2008)
119. Gonoskov A A et al. *Phys. Rev. Lett.* **102** 184801 (2009)
120. Naumova N et al. *Phys. Rev. Lett.* **102** 025002 (2009)
121. Schlegel T et al. *Phys. Plasmas* **16** 083103 (2009)
122. Sinha U, Kaw P *Phys. Plasmas* **19** 033102 (2012)
123. Bulanov S V et al. *Phys. Plasmas* **19** 103105 (2012)
124. Landau L D, Lifshitz E M *The Classical Theory of Fields* (Oxford: Butterworth-Heinemann, 1980); Translated from Russian: *Teoriya Polya* (Moscow: Nauka, 1988)
125. Peano F et al. *IEEE Trans. Plasma Sci.* **36** 1857 (2008)
126. Salamin Y I, Harman Z, Keitel C H *Phys. Rev. Lett.* **100** 155004 (2008)
127. Salamin Y I et al. *Phys. Rev. A* **85** 063831 (2012)
128. Li J-X et al. *Phys. Rev. A* **85** 063832 (2012)
129. Berezin Yu A, Vshivkov V A *Metod Chastits v Dinamike Razrezhennoi Plazmy* (Particle Method in the Dynamics of a Rarefied Plasma) (Novosibirsk: Nauka, 1980)
130. Hockney R W, Eastwood J W *Computer Simulation Using Particles* (New York: McGraw-Hill, 1981)
131. Andreev A A et al. *Plasma Phys. Control. Fusion* **48** 1605 (2006)
132. Esirkepov T Zh et al. *Nucl. Instrum. Meth. Phys. Res. A* **745** 150 (2014)
133. Paradkar B S, Krasheninnikov S I, Beg F N *Phys. Plasmas* **19** 060703 (2012)
134. Robinson A P L, Arefiev A V, Neely D *Phys. Rev. Lett.* **111** 065002 (2013)
135. Last I, Schek I, Jortner J *J. Chem. Phys.* **107** 6685 (1997)
136. Nishihara K et al. *Nucl. Instrum. Meth. Phys. Res. A* **464** 98 (2001)
137. Kovalev V F, Bychenkov V Yu *Phys. Rev. Lett.* **90** 185004 (2003)
138. Bychenkov V Yu, Kovalev V F *Plasma Phys. Rep.* **31** 178 (2005); *Fiz. Plazmy* **31** 203 (2005)
139. Murakami M, Basko M M *Phys. Plasmas* **13** 012105 (2006)
140. Krainov V P, Smirnov M B *Phys. Rep.* **370** 237 (2002)
141. Echkina E Y et al. *Laser Phys.* **19** 228 (2009)
142. Sakabe S et al. *Phys. Rev. A* **69** 023203 (2004)
143. Askar'yan G A, Bulanov S V *Sov. Tech. Phys. Lett.* **9** 533 (1983); *Pis'ma Zh. Tekh. Fiz.* **9** 1243 (1983)
144. Kumarappan V, Krishnamurthy M, Mathur D *Phys. Rev. Lett.* **87** 085005 (2001)
145. Zigler A et al. *Phys. Rev. Lett.* **110** 215004 (2013)
146. Echkina E Y et al., in *31st European Physical Society Conf. on Plasma Physics, London, 28 June – 2 July 2004* (Europhysics Conf. Abstracts, Vol. 28G, Eds P Norreys, H Hutchinson) (London: EPS, 2004) P-2.032
147. Esirkepov T Zh *Comput. Phys. Commun.* **135** 144 (2001)
148. Kaplan A E, Dubetsky B Y, Shkolnikov P L *Phys. Rev. Lett.* **91** 143401 (2003)
149. Peano F, Fonseca R A, Silva L O *Phys. Rev. Lett.* **94** 033401 (2005)
150. Wilks S C et al. *Phys. Rev. Lett.* **69** 1383 (1992)
151. Passoni M et al. *Phys. Rev. E* **69** 026411 (2004)
152. Mora P *Phys. Rev. Lett.* **90** 185002 (2003)
153. Kiefer T, Schlegel T *Phys. Plasmas* **19** 102101 (2012)
154. Kiefer T, Schlegel T, Kaluza M C *Phys. Rev. E* **87** 043110 (2013)
155. Hau L-N, Fu W-Z *Phys. Plasmas* **14** 110702 (2007)
156. Hellberg M A et al. *Phys. Plasmas* **16** 094701 (2009)
157. Gurevich A V, Pariiskaya L V, Pitaevskii L P *Sov. Phys. JETP* **22** 449 (1966); *Zh. Eksp. Teor. Fiz.* **49** 647 (1965)

158. Allen J E, Andrews J G *J. Plasma Phys.* **4** 187 (1970)
159. Crow J E, Auer P L, Allen J E *J. Plasma Phys.* **14** 65 (1975)
160. Denavit J *Phys. Fluids* **22** 1384 (1979)
161. Gurevich A V, Meshcherkin A P *Sov. Phys. JETP* **53** 937 (1981); *Zh. Eksp. Teor. Fiz.* **80** 1810 (1981)
162. Gurevich A V, Meshcherkin A P *Sov. J. Plasma Phys.* **8** 283 (1982); *Fiz. Plazmy* **8** 502 (1982)
163. Medvedev Yu V *Plasma Phys. Control. Fusion* **53** 125007 (2011)
164. Tikhonchuk V T et al. *Plasma Phys. Control. Fusion* **47** B869 (2005)
165. Landau L D, Lifshitz E M *Fluid Mechanics* (Oxford: Pergamon Press, 1987); Translated from Russian: *Gidrodinamika* (Moscow: Nauka, 1982)
166. Mako F, Tajima T *Phys. Fluids* **27** 1815 (1984)
167. Yu W et al. *Phys. Rev. Lett.* **85** 570 (2000)
168. Arefiev A V et al. *Phys. Rev. Lett.* **108** 145004 (2012)
169. Bulanov S V, Kovrizhnykh L M, Sakharov A S *Phys. Rep.* **186** 1 (1990)
170. Bulanov S V, Naumova N M, Pegoraro F *Phys. Plasmas* **1** 745 (1994)
171. D'yachenko V F, Imshennik V S *Sov. J. Plasma Phys.* **5** 413 (1979); *Fiz. Plazmy* **5** 737 (1979)
172. Brunel F *Phys. Rev. Lett.* **59** 52 (1987)
173. Veksler V I *Sov. J. Atom. Energy* **2** 525 (1957); *At. Energ.* **2** 427 (1957)
174. Bulanov S V et al. *Phys. Usp.* **56** 429 (2013); *Usp. Fiz. Nauk* **183** 449 (2013)
175. Bulanov S V et al. *Phys. Plasmas* **17** 063102 (2010)
176. Bulanov S S et al. *Phys. Plasmas* **19** 093112 (2012)
177. Bulanov S S et al., arXiv:1310.8019
178. Macchi A, Veghini S, Pegoraro F *Phys. Rev. Lett.* **103** 085003 (2009)
179. Bulanov S V et al. *Phys. Rev. Lett.* **104** 135003 (2010)
180. Vshivkov V A et al. *Phys. Plasmas* **5** 2727 (1998)
181. Bulanov S S et al. *Phys. Rev. E* **78** 026412 (2008)
182. Bulanov S S et al. *Med. Phys.* **35** 1770 (2008)
183. Morita T et al. *J. Phys. Soc. Jpn.* **81** 024501 (2012)
184. Litvak A G *Sov. Phys. JETP* **30** 344 (1970); *Zh. Eksp. Teor. Fiz.* **57** 629 (1969)
185. Bulanov S S et al. *Phys. Plasmas* **17** 043105 (2010)
186. Sun G-Z et al. *Phys. Fluids* **30** 526 (1987)
187. Sandhu A S et al. *Phys. Rev. Lett.* **89** 225002 (2002)
188. Wagner U et al. *Phys. Rev. E* **70** 026401 (2004)
189. Amitani H et al. *AIP Conf. Proc.* **611** 340 (2002)
190. Willingale L et al. *Phys. Rev. Lett.* **98** 049504 (2007)
191. Sylla F et al. *Phys. Rev. Lett.* **110** 085001 (2013)
192. Matsukado K et al. *Phys. Rev. Lett.* **91** 215001 (2003)
193. Yogo A et al. *Phys. Rev. E* **77** 016401 (2008)
194. Sagdeev R Z, in *Reviews of Plasma Physics* Vol. 4 (Ed. M A Leontovich) (New York: Consultants Bureau, 1966) p. 23; Translated from Russian: in *Voprosy Teorii Plazmy* Iss. 4 (Ed. M A Leontovich) (Moscow: Gosatomizdat, 1964) p. 20
195. Biskamp D *Nucl. Fusion* **13** 719 (1973)
196. Haberberger D et al. *Nature Phys.* **8** 95 (2012)
197. Fiuza F et al. *Phys. Rev. Lett.* **109** 215001 (2012)
198. Leemans W P et al. *AIP Conf. Proc.* **1299** 3 (2010)
199. Kiriyama H et al. *Appl. Sci.* **3** 214 (2013)
200. Mourou G et al. *Nature Photon.* **7** 258 (2013)
201. Mourou G, private communication
202. Krushelnick K et al. *IEEE Trans. Plasma Sci.* **28** 1184 (2000)
203. Roth M et al. *Phys. Rev. Lett.* **86** 436 (2001)
204. Bychenkov V Yu et al. *Plasma Phys. Rep.* **27** 1017 (2001); *Fiz. Plazmy* **27** 1076 (2001)
205. Atzeni S, Temporal M, Honrubia J J *Nucl. Fusion* **42** L1 (2002)
206. Honrubia J J et al. *Phys. Plasmas* **16** 102701 (2009)
207. Gus'kov S Yu *Plasma Phys. Rep.* **39** 1 (2013); *Fiz. Plazmy* **39** 3 (2013)
208. Kawata S et al. *Laser Therapy* **22** 103 (2013)
209. Humphries S (Jr.) *Charged Particle Beams* (New York: Wiley, 1990)
210. Kapchinskii I M *Dinamika Chastits v Lineinykh Rezonansnykh Uskoritelyakh* (Particle Dynamics in Linear Resonance Accelerators) (Moscow: Atomizdat, 1966)
211. Lichtenberg A J *Phase-Space Dynamics of Particles* (New York: Wiley, 1969); Translated into Russian: *Dinamika Chastits v Fazovom Prostranstve* (Moscow: Atomizdat, 1972)
212. Schollmeier M et al. *Phys. Rev. Lett.* **101** 055004 (2008)
213. Nishiuchi M et al. *Appl. Phys. Lett.* **94** 061107 (2009)
214. Harres K et al. *Phys. Plasmas* **17** 023107 (2010)
215. Roth M et al. *Plasma Phys. Control. Fusion* **51** 124039 (2009)
216. Burris-Mog T et al. *Phys. Rev. ST Accel. Beams* **14** 121301 (2011)
217. Sinigardi S et al. *Phys. Rev. ST Accel. Beams* **16** 031301 (2013)
218. Bulanov S V, Mourou G, Tajima T *Phys. Lett. A* **372** 4813 (2008)
219. Toncian T et al. *Science* **312** 410 (2006)
220. Kar S et al. *Phys. Rev. Lett.* **100** 105004 (2008)
221. Nishiuchi M et al. *Phys. Plasmas* **19** 030706 (2012)
222. Toncian T et al. *AIP Adv.* **1** 022142 (2011)
223. Noda A et al. *Laser Phys.* **16** 647 (2006)
224. Noda A et al. *Int. J. Mod. Phys. B* **21** 319 (2007)
225. Nakamura S et al. *Jpn. J. Appl. Phys.* **46** L717 (2007)
226. Garoby R, arXiv:1112.3232; CERN Yellow Report CERN-2011-007 (Ed. R Bailey) (Geneva: CERN, 2012) p. 431
227. Ruhl H et al. *Plasma Phys. Rep.* **27** 363 (2001); *Fiz. Plazmy* **27** 387 (2001)
228. Qiao B et al. *Phys. Rev. E* **87** 013108 (2013)
229. Kawata S et al. *J. Phys. Conf. Ser.* **112** 042044 (2008)
230. Kawata S et al. *IEEE Trans. Plasma Sci.* **36** 363 (2008)
231. Roth M et al. *Phys. Rev. ST Accel. Beams* **5** 061301 (2002)
232. Patel P K et al. *Phys. Rev. Lett.* **91** 125004 (2003)
233. Snavely R A et al. *Phys. Plasmas* **14** 092703 (2007)
234. Bartal T et al. *Nature Phys.* **8** 139 (2011)
235. Keldysh L V *Sov. Phys. JETP* **20** 1307 (1965); *Zh. Eksp. Teor. Fiz.* **47** 1945 (1964)
236. Popov V S *Phys. Usp.* **47** 855 (2004); *Usp. Fiz. Nauk* **174** 921 (2004); Karnakov B M, Mur V D, Popruzhenko S V, Popov V S *Phys. Usp.* **58** 1 (2015), http://dx.doi.org/10.3367/UFNe.0185.201501b.0003; *Usp. Fiz. Nauk* **185** 3 (2015)
237. Fuchs J et al. *Nature Phys.* **2** 48 (2006)
238. Pfotenhauer S M et al. *New J. Phys.* **10** 033034 (2008)
239. Margarone D et al. *Phys. Rev. Lett.* **109** 234801 (2012)
240. Floquet V et al. *J. Appl. Phys.* **114** 083305 (2013)
241. Esirkepov T, Yamagiwa M, Tajima T *Phys. Rev. Lett.* **96** 105001 (2006)
242. d'Humières E et al. *Phys. Plasmas* **20** 023103 (2013)
243. Morace A et al. *Appl. Phys. Lett.* **103** 054102 (2013)
244. Morita T et al. *Phys. Rev. Lett.* **100** 145001 (2008)
245. Yogo A *Rev. Laser Eng.* **40** 842 (2012)
246. Luo W et al. *Med. Phys.* **32** 794 (2005)
247. Downs J A et al. *Nature* **447** 951 (2007)
248. Folkard M et al. *Int. J. Radiat. Biol.* **69** 729 (1996)
249. Furusawa Y et al. *Radiat. Res.* **154** 485 (2000)
250. Douglas B G, Fowler J F *Radiat. Res.* **66** 401 (1976)
251. Bortfeld T, Jeraj R *Br. J. Radiol.* **84** 485 (2011)
252. Charatis G J et al., in *Plasma Physics and Controlled Nuclear Fusion Research, Intern. Conf.* Vol. 2 (Vienna: IAEA, 1975) p. 317
253. Gitomer S J et al. *Phys. Fluids* **29** 2679 (1986)
254. Clark E L et al. *Phys. Rev. Lett.* **84** 670 (2000)
255. Maksimchuk A et al. *Phys. Rev. Lett.* **84** 4108 (2000)
256. Snavely R A et al. *Phys. Rev. Lett.* **85** 2945 (2000)
257. Fritzler S et al. *Appl. Phys. Lett.* **83** 3039 (2003)
258. Maksimchuk A et al. *Appl. Phys. Lett.* **102** 191117 (2013)
259. Bulanov S V, Khoroshkov V S, News Lett. NEPC, 29 Jan. (2002) p. 10
260. Bulanov S V, Khoroshkov V S *Med. Fiz.* (1(13)) 50 (2002)
261. Sheng Z-M et al. *Phys. Rev. Lett.* **85** 5340 (2000)
262. Morita T et al. *Phys. Plasmas* **16** 033111 (2009)
263. Bert C, Engenhart-Cabillic R, Durante M *Med. Phys.* **39** 1716 (2012)
264. Ganz J C *Gamma Knife Neurosurgery* (Wien: Springer-Verlag, 2011)
265. Nakamura T et al. *Phys. Rev. Lett.* **108** 195001 (2012)
266. Ridgers C P et al. *Phys. Rev. Lett.* **108** 165006 (2012)
267. Bulanov S V et al. *Proc. SPIE* **8780** 878015 (2013)